Journal of Medicinal Chemistry

Structural modification of natural product ganomycin I leading to discovery of a #-glucosidase and HMG-CoA reductase dual inhibitor improving obesity and metabolic dysfunction in vivo

Kai Wang, Li Bao, Nan Zhou, Jinjin Zhang, mingfang Liao, Zhongyong Zheng, Yujing Wang, Chang Liu, Jun Wang, Lifeng Wang, Wenzhao Wang, Shuang-Jiang Liu, and Hongwei Liu

J. Med. Chem., **Just Accepted Manuscript** • DOI: 10.1021/acs.jmedchem.8b00107 • Publication Date (Web): 10 Apr 2018

Just Accepted

ACS Publications

is published by the American Chemical Society. 1155 Sixteenth Street N.W., Washington, DC 20036

Structural modification of natural product ganomycin I leading to discovery of a α-glucosidase and HMG-CoA reductase dual inhibitor improving obesity and metabolic dysfunction *in vivo*

Kai Wang, [a,b,⊥] Li Bao, [a, b, ⊥] Nan Zhou, [c] Jinjin Zhang, [a,b] Mingfang Liao,[a,b]

Zhongyong Zheng , [a,b] Yujing Wang , [b,c] Chang Liu , [c] Jun Wang , [d] Lifeng Wang, [e]

Wenzhao Wang, [a] ShuangJiang Liu , [b,c] Hongwei Liu [a, b, *]

[a] *State Key Laboratory of Mycology, Institute of Microbiology, Chinese Academy of Sciences, No.1 Beichenxi Road, Chaoyang District, Beijing 100101, P. R. China*

[b] *University of Chinese Academy of Sciences, Beijing, 100049, P. R. China*

[c] *State Key Laboratory of Microbial Resources, Institute of Microbiology, Chinese Academy of Sciences, No.1 Beichenxi Road, Chaoyang District, Beijing 100101, P. R. China*

[d] *CAS Key Laboratory of Pathogenic Microbiology and Immunology, Institute of Microbiology, Chinese Academy of Sciences, No.1 Beichenxi Road, Chaoyang District, Beijing 100101, P. R. China*

[e] *Beijing Kangyuan Pharmaceutical Co., Ltd., No. 3 Changliu Road, Changping District, 102200, Beijing P. R. China*

---

[a] State Key Laboratory of Mycology, Institute of Microbiology

[b] University of Chinese Academy of Sciences.

[c] State Key Laboratory of Microbial Resources, Institute of Microbiology

[d] CAS Key Laboratory of Pathogenic Microbiology and Immunology, Institute of Microbiology

[e] Beijing Kangyuan Pharmaceutical Co., Ltd.

[⊥] K. Wang, L. Bao contributed equally to this article.

* Corresponding Author Tel: +86 10 64806074; E-mail: liuhw@im.ac.cn (H-W, Liu)

Abstract: It is a great challenge to develop drugs for treatment of metabolic syndrome. With ganomycin I as a leading compound, fourteen meroterpene derivatives were synthesized and screened for their α-glucosidase and HMG-CoA reductase inhibitory activities. As a result, a α-glucosidase and HMG-CoA reductase dual inhibitor ((R,E)-5-(4-(tert-butyl)phenyl)-3- (4,8-dimethylnona-3, 7-dien-1-yl) furan-2(5H)-one， **7d**) with improved chemical stability and long-term safety was obtained. Compound **7d** showed multiple and strong *in vivo* efficacies in reducing weight gain, lowering HbAlc level, and improving insulin resistance and lipid dysfunction in both *ob/ob* and diet-induced obesity (DIO) mice models. Compound **7d** was also found to reduce hepatic steatosis in *ob/ob* model. 16S rRNA gene sequencing, SCFA and intestinal mucosal barrier function analysis indicated that gut microbiota plays a central and causative role in mediating of the multiple efficacies of **7d**. Our results demonstrate that **7d** is a promising drug candidate for metabolic syndrome.

Introduction

Metabolic syndrome (MS) has become an important public health issue worldwide. [1] Take China as an example, it was estimated that 454 million adults were suffering from MS diseases in 2010. [2] MS is a polygenetic, multi-organ disease characterized by insulin resistance, central obesity, elevated blood pressure, dyslipidemia, and nonalcoholic steatohepatitis (NASH). The polypharmacology strategy by a multitude of drugs for treating multifactorial diseases is unfavorable due to the complex and problematic drug-drug interactions and additional side effects in clinics. [3] An ideal anti-MS drug should address the multitude of the desired therapeutic targets and exhibit multiple effects in lowering blood glucose and plasma lipid levels, reducing body weight, and improving cardiovascular health. Natural products with diverse bioactivity-related scaffolds and pharmacophore patterns are often recognized with multi-effects. [4, 5] Recently, withaferin A, a steroidal lactone from *Withania somnifera*, has been identified as potential candidate with multiple metabolic benefits of the body-weight loss, the reduced hepatic steatosis, and the antidiabetic action. [6]

The enzyme 3-hydroxy-3-methylglutaryl co-enzyme A reductase (HMG-CoA reductase) catalyzes the conversion of HMG-CoA to mevalonate, a key precursor of cholesterol biosynthesis. [7] Statins, which decrease the level of plasma cholesterol through inhibiting HMG-CoA reductase, represent the major class of hypolipidemic drugs in clinics. [8] The enzyme α-glucosidase in the brush border of the intestinal epithelial cells is a well-known target for the development of anti-diabetic drugs. α-Glucosidase inhibitors (AGIs: acarbose, miglitol, voglibose) can retard the digestion

and absorption of carbohydrates in the small intestine, and thus reducing postprandial hyperglycemia and delaying the development of type 2 diabetes in patients. [9] The involvement of the gut microbiota in host health and pathogenesis of metabolic diseases have been demonstrated. [10] A 'microbiota-to-host paradigm' has been recommended as a new strategy for the development of new drugs or therapeutic approaches for the treatment metabolic diseases. [11, 12] The inhibition of α-glucosidase by AGIs accumulates more undigested carbohydrates in the lower parts of the gut, [13] which alteres gut microbial fermentation and further modulates the composition and function of gut microbiota. [14-16] Medicines (metformin, [17] berberine, [18, 19] acarbose, and obeticholic acid [20] or diet supplemented with plant extracts or plant-derived components [21, 22] have shown cures and/or prevention of metabolic diseases through modulating of gut microbiota. In light of the hypolipidemic efficacy of HMG-CoA reductase inhibitor and the hypoglycemic and gut microbiota modulation effect of α-glucosidase inhibitor, a dual inhibitor of HMGCR and α-glucosidase could be a promising drug candidate to treat metabolic syndrome.

Ganoderma species (Ganodermataceae, Polyporales) are well-known as elixir in China, and being widely used as functional foods and traditional medicine in Asian countries. [23] Ganomycin I, a meroterpene-type and dual inhibitor of both *α*-glucosidase and HMG-CoA reductase from *Ganoderma* spp., was found to possess hypoglycemic, hypolipidemic, and insulin-sensitizing effects on KK-A^y mice in our early work. [24] However, the *para*-dihydroxylbenzene moiety in its structure disadvantages the further drug development due to its chemical instability. Herein, we

synthesized fourteen ganomycin I derivatives and screened for their *in vitro* α-glucosidase and HMG-CoA reductase inhibitory acitivities. As a result, a new dual inhibitor (R,E)-5-(4-(tert-butyl)phenyl)-3-(4,8-dimethylnona-3,7-dien-1-yl) furan- 2 (5H)-one (**7d**) with good stability and high potency was obtained. Compound **7d** exhibited multiple and potent anti-MS efficacies by a combination of the hypoglycemic, hypolipidemic, and weight control activities in both *ob/ob* and DIO mice. In addition, gut microbiota was confirmed to play a central role in mediating the therapeutic effects of **7d**.

Results and Discussion

Chemistry. It was observed that ganomycin I slowly decomposed after two-weeks exposure at room temperature due to its hydroquinone structural feature. To search for new meroterpene derivatives with good stability and strong bioactivity, fourteen ganomycin I analogues with different aromatic groups were synthesized. The synthetic routes were developed by modifications of the reported synthetic method for ganomycin I (Scheme 1). [25] In brief, the key vinylbenzyl alcohols (**2a**-**2l**) were synthesized from commercially available benzaldehyde analogues (**1a-1l**) by the grignard reaction, and then transformed into **3a**-**3l** by manganese dioxide and Corey-Bakshi-Shibata (CBS) reduction. Compound **6** was prepared from geraniol (**4**) as previously reported. [25] Compounds **3a**-**3l** and **6** were respectively connected, and further converted into analogues by the same method as described for ganomycin I. Compound **7m** was prepared from **7l** by hydrolysis. Compound **7n** was synthesized in

a similar manner as described above with naphthaldehyde **1n** as starting material. (Scheme S1).

Bioactivity Screening. The activities of analogues **7a-7n** against both HMG-CoA reductase from pig liver microsomes and α-glucosidase from rat small intestinal mucosa were shown in Table 1. Ganomycin I, atorvastatin, and acarbose were used as reference compounds. Compounds **7a-7n** inhibited HMG-CoA reductase in a concentration dependent manner with IC_{50} in the range between 5.82 and 112.12 μM. As to the inhibitory activity against α-glucosidase , compounds **7b**, **7c**, **7d** and **7f** showed much stronger activity than ganomycin I. The structure of **7e** is quite similar to that of **7d**, but it showed much weaker activities in both HMG-CoA reductase and α-glucosidase assays than **7d**. To further verify the biossay results, the α-glucosidase inhibitory activity of **7c**, **7d**, **7e**, and **7f** was determined by another detection method using high performance liquid chromatrography. As a result, the IC_{50} values of **7c**, **7d**, **7e**, and **7f** were determined to be 0.23, 0.04, 28.66, 0.16 μM, respectively, similar to those obtained by colorimetry (Figure S1). Therefore, a deep structure-activity relationship analysis needs further investigation. (R,E)-5-(4-(tert-butyl)phenyl) -3-(4,8-dimethylnona-3,7-dien-1-yl)furan-2(5H)-one (**7d**) displaying the strongest activities against both α-glucosidase and HMG-CoA reductase (with a 6.3-fold and 2.1-fold stronger than ganomycin I respectively) was selected for *in vivo* study.

Stability and toxicity of 7d. In chemical stability assay, compound **7d** showed a better chemical stability than Ganomycin I when exposed under room temperature (Figure S2). Compound **7d** was also confirmed to be safe by a long-term safety assay.

Daily oral administration of 30.0 mg/kg of **7d** for 90 days showed no negative effects on behavior, body weight, blood glucose, liver function, organ coefficients, or survival (Figure S3).

***In vivo* PK Profile of 7d.** Compound **7d** was further investigated for the pharmacokinetic (PK) properties (via p.o. route, with 2.0 mg/kg in SD rat). The mean plasma concentration-time curve of **7d** after intragastric administration in rats is shown in Figure S4. The relevant pharmacokinetic parameters are listed in Table 2. Compound **7d** showed a half-life of 1.8 h, an AUC of 280.2 ng/mL × h, and a C_{max} of 49.3 ng/mL.

***In vivo* efficacy.** We used *ob/ob* diabetic and DIO (C57BL/*6J*) mice to evaluate the hypoglycemic and hypolipidemic effects for **7d**. Acarbose, the *α*-glucosidase inhibitor used in clinics, was used as positive controls in *ob/ob* mice assay. Compound **7d** (0.3 mg/kg, 1.0 mg/kg and 3.0 mg/kg) was daily administered by gavage method.

The *ob/ob* mice treated with 3.0 mg/kg of **7d** showed a 68% reduction in weight gain, as compared to that of the vehicle-treated *ob/ob* group (2.0 g per mouse versus 6.5 g per mouse, respectively; Figure 1A). Moreover, the cumulative food intake for 25 days in the compound **7d**-treated group (3.0 mg/kg) was decreased to 78% of the vehicle-treated *ob/ob* group (Figure 1B). The LEE index and absolute fat mass in compound **7d**-treated mice were also reduced substantially (Figures 1C, D), whereas the lean mass was changed slightly (Figure 1E). In a separate experiment with DIO mice, compound **7d** treatment led to a 25.4% reduction in body weight (Figures S5),

as compared with that of the vehicle-treated group. The positive control, acarbose, showed weak effects on body weight gain, cumulative food intake, and LEE index.

In addition, *ob/ob* mice treated with compound **7d** (at 0.3, 1.0 and 3.0 mg/kg) showed dose-dependent decreases in fasting blood glucose, free diet blood glucose, and glycated hemoglobin A1c (HbA1c) levels (Figures 2A-C). Compound **7d** treatment also improved glucose tolerance and insulin resistance, and significantly enhanced the insulin sensitivity index (ISI; Figure 2D). The mean area under curves (AUC) during the oral glucose tolerance test (OGTT) and the insulin tolerance test (ITT) of **7d**-treated *ob/ob* mice was much lower than that of the vehicle-treated mice (Figures 2E-H). DIO mice treated with **7d** produced similar effects on glucose tolerance and insulin resistance as those observed in *ob/ob* mice (Figures S6).

Treating the *ob/ob* mice with **7d** also decreased levels of serum total cholesterol (TC), free fatty acids (FFAs), and triglycerides (TG) in a dose dependent manner (Figures 3A-C). Particularly, the serum TG level in compound **7d**-treated mice (3.0 mg/kg) was decreased to 47% of the vehicle-treated *ob/ob* mice (Figure 3B). Compound **7d** treatment at the 1.0 mg/kg and 3.0 mg/kg doses also caused reductions of 43% and 51% in the LDL-C levels of *ob/ob* mice, respectively, as compared with that of the vehicle-treated group (Figure 3A). In recent studies, a group of low-density-lipoprotein-cholesterol (LDL-C)-reducing medicines have been proved to be effective at treating dyslipidemia in clinical trials. [26-28] Examination of hematoxylin-eosin (H&E)-stained sections of white adipose tissue (WAT) indicated the presence of macrovesicular steatosis in *ob/ob* mice. Compound **7d** (3.0 mg/kg)

effectively reduced the size of the adipocytes in WAT (Figures 3D, E). DIO mice exhibited similar improvements on lipid metabolism as *ob/ob* mice under the oral treatment of **7d** (Figures S7).

Steatosis and nonalcoholic steatohepatitis (NASH) commonly accompany with obesity and the obesity-related metabolic disorders. [29] We found that compound **7d** reduced levels of FFAs, TG, TC, and LDL-C in the livers of *ob/ob* mice (Figures 4A-C) and decreased the activities of serum alanine aminotransferase (ALT) and aspartate transaminase (AST; Figures 4D, E). In addition, compound **7d** administered at 3.0 mg/kg apparently reduced macrosteatosis, hepatocyte ballooning, and fat deposition in the livers of *ob/ob* mice, as indicated by liver sections staining and microscopy observation (Figure 4H). Compound **7d** (3.0 mg/kg) also decreased hepatic hydroxyproline levels, TGF-β1 (a pro-fibrogenic protein) expression, and liver fibrosis (Figures 4F-H). These results support the effectiveness of **7d** in reducing hepatic steatosis and liver fibrosis.

Overall, compound **7d** has been demonstrated so far to be a potential drug candidate with multiple therapeutic effects including the reduction of weight gain, the hypoglycemic and hypolipidemic actions, and the improvement of hepatic steatosis and fibrosis. Compound **7d** exhibited more potency than ganomycin I in lowering body weight gain, and similar efficacies with that of ganomycin I in improving hyperglycemia and hyperlipidemia (Figure S5-S7).

Mechanism study. The *in vivo* inhibitory effect of **7d** on *α*-glucosidase was confirmed by the oral sucrose tolerance test (OSTT) and oral maltose tolerance test

(OMTT) in both *ob/ob* mice and diet induced obesity (DIO) (Figures 5A-D and Figures S8A-D). The administration of sucrose or maltose (4 g/kg of body weight, p.o.) to the fasted mice resulted in a rapid increase in blood glucose concentrations after 40 min, and then blood glucose was recovered to the pretreatment level at 120 min. Treatment of **7d** (at 0.3, 1.0 and 3.0 mg/kg) and acarbose induced a significant reduction of blood glucose levels at 40, 80 and 120 min when compared with that of the model group (Figures 5A-D).

As a potent α-glucosidase inhibitor, treatment with **7d** at a dose of 3.0 mg/kg accumulated more carbohydrates in the lower parts of the small intestine (Figure S8E) in *ob/ob* mice, which may alter the composition and function of gut microbiota. To evaluate the influence of **7d** on gut microbiota, we investigated the composition and abundance of gut microbiota by high-throughput sequencing (Hiseq) of the V3-V4 hypervariable region of the 16S rDNA genes from the caecum contents of mice and performed comparative analysis between the vehicle-treated and compound **7d**-treated groups (at 1.0 and 3.0 mg/kg). The composition and abundance of gut microbiota from the compound **7d**-treated *ob/ob* mice significantly differed from that of vehicle-treated *ob/ob* mice (NMDS plot, MRPP test, $p = 0.001$; Figures 6A, B). The analysis with linear discriminant analysis (LDA) effect size (LEfSe) method revealed a significant increase in Lachnospiraceae in compound **7d**-treated mice, accompanying with the decrease of Alphaproteobacteria, Betaproteobacteria, and Gammaproteobacteria (Figure 6C). Members of Lachnospiraceae were reported to generate short-chain fatty acids (SCFAs) from polysaccharides by fermentation. [30]

The increased level of gut butyrate in **7d**-treated mice (at a dose of 3.0 mg/kg) was further confirmed by GC-MS analysis of SCFAs in mice feces (Figures 7A, B).

Metabolic endotoxemia (low-grade elevation in plasma LPS) has been regarded as the major cause for the initiation of obesity and obesity-related dysfunctions. [31] Increases in lipopolysaccharide (LPS)-producing gut bacteria or the occurrence of gut dysbiosis can trigger the state of metabolic endotoxemia. [31, 32] It was found that the abundance of LPS-producing bacteria in the genus of *Neisseri*, *Prevotella*, *Fusobacterium,* and *Selenomonas,* [33, 34] *and* the pro-inflammatory bacteria in the genus of *Alistipes* and *Oscillibacter* [35-37] was markedly reduced in the gut of **7d**-treated mice (Figure 6D). In accordance with above analysis, compound **7d** treatment at doses of 1.0 mg/kg and 3.0 mg/kg led to 29.8% and 40.9% reduction of plasma LPS in *ob/ob* mice, respectively (Figure 7C), as compared with that in the vehicle-treated group. Meanwhile, treatment of compound **7d** at a dose of 3.0 mg/kg significantly reduced the level of TNF-α, an important inflammatory factor stimulated by LPS (Figure 7D). Immunofluorescence analysis confirmed the reduced expression of TNF-α in the liver of **7d** treated mice (3.0 mg/kg; Figures 7E, F). RNA-seq analysis of differentially expressed genes in liver also demonstrated reduced systemic inflammation in the compound **7d**-treated mice (3.0 mg/kg). Gene-ontology (GO)-based functional annotation analysis of all downregulated and differentially expressed genes (≥ 2-fold) indicated that the top 10 enriched biological processes correlated with inflammation and immunity (Figure S9A). A Kyoto Encyclopaedia of Genes and Genomes (KEGG) analysis of these genes further indicated that 14 of the

top 20 pathways were involved in the inflammatory response and autoimmunity (e.g. Fc-γ-receptor-mediated phagocytosis, type 1 diabetes mellitus, leishmaniasis, tuberculosis, asthma, inflammatory bowel disease (IBD), and rheumatoid arthritis; Figure S9B).

Butyrate produced by intestinal bacteria plays significant physiological roles in stimulating mucin release, enhancing mRNA expression of mucosal integrity proteins [38, 39] and tight junction proteins, [40] and improving the energy metabolism. [41] We investigated the effects of **7d** on intestinal inflammation and mucosal barrier function in *ob/ob* mice. Results indicated that treatment with **7d** at a dose of 3.0 mg/kg decreased the mRNA expression of pro-inflammatory cytokine TNF-α and increased the mRNA expression of anti-inflammatory cytokine IL-10, mucosal integrity proteins (Muc-1 and Muc-5), and tight junction proteins (ZO-1 and Occludin) in the ileum (Figure 7G). Butyrate also participates in the maintenance of gut homeostasis. [42] It prevents dysbiotic expansion of Gram-negative bacteria by limiting oxygen or nitrate supply to these bacteria via butyrate-activated PPAR-γ signaling. The activation of epithelial PPAR-γ signaling by butyrate subsequently enhances *β*-oxidation of fatty acids and reduces epithelial expression of *Nos2*. We found that treatment with **7d** at a dose of 3.0 mg/kg upregulated mRNA expression of *Pparg* and downregulated mRNA expression of the inducible nitric oxide synthase gene *Nos2* in epithelial colonocytes (Figure 7H). We also detected decreased nitrate levels in the colonic lumen of **7d**-treated ob/ob mice (3.0 mg/kg; Figure 7I). Thus, the enhanced level of butyrate by **7d** due to the increase of Lachnospiraceae in gut microbiota is conductive to

improving gut barrier function and preventing the expansion of Gram-negative Proteobacteria.

Finally, we conducted experiments with pseudo-germ-free *ob/ob* mice to further confirm the role of gut microbiota in mediating the effects of **7d**. Pseudo-germ-free mice were generated by administering a cocktail of broad-spectrum antibiotics (ampicillin, vancomycin, neomycin, gentamycin, and erythromycin) to *ob/ob* mice for three weeks (Figure S10). Antibiotics pretreatment largely decreased the therapeutic efficacies of **7d** (at a dose of 3.0 mg/kg) on ameliorating endotoxemia, reducing weight gain and food intake, and improving blood glucose and lipid metabolic disorders in *ob/ob* mice (Figure S11). Interestingly, Abx-treatment could not completely abolish the hypolipidemic effects of **7d**. Compound **7d** treatment significantly decreased the plasma TG level and the weight gain as compared to that of the vehicle-treated Abx group (Figure S11), which might be attributed to the inhibitory activity of **7d** against HMG-CoA reductase. Atorvastatin and rosuvastatin have been reported to reduce body weight gain, improve diabetes-related metabolic disorders, and alleviate inflammation. [43] Together, these data indicated that the therapeutic effects of **7d** are largely dependent on its modulation on gut microbiota.

Conclusion.

With natural product ganomycin I as a leading compound, fourteen meroterpene derivatives (**7a**-**7n**) were synthesized and screened for their *in vitro* HMG-CoA reductase and α-glucosidase inhibitory activities. A potent dual inhibitor **7d** with good chemical stability, long-term safety, and multiple *in vivo* beneficial effects was

obtained. Compound **7d** exhibited multi-effects in reducing weight gain, lowering HbAlc level, and improving insulin resistance, lipid dysfunction and hepatic steatosis. It was demonstrated that **7d** exerted its therapeutic effects through modulation of gut microbiota. The changed gut microbiota enhanced the level of gut SCFAs (butyrate and propionate) and restored intestinal mucosal barrier function, which consequently reduced the metabolic endotoxemia. The worldwide epidemic of obesity and the related metabolic diseases have become a serious public health problem. The current work confirms that the new concept of "microbiota to host paradigm" for the treatment of metabolic diseases is reasonable and promising.

Experimental Section

Chemistry

Reagents and Methods. All commercial chemicals and solvents are reagent grade and were used without further purification unless otherwise noted. All reactions are stirred magnetically. Solvents used for extraction and chromatographic separation were analytical grade. TLC was carried out on silica gel HSGF254, and the spots were visualized by spraying with 10% H_2SO_4 and heating. Silica gel (Qingdao Haiyang Chemical Co., Ltd., People's Republic of China). HPLC analysis was performed on an Agilent 1200 HPLC system using the YMC-Pack ODS column (C18, 250 × 4.6 mm, 5 μm) with DAD detector at a flow rate of 1.0 mL/min. UV and IR spectral data were acquired using a Thermo Genesys-10S UV−vis and Nicolet IS5FT-IR spectrophotometer, respectively. Specific rotations were recorded on a PerkinElmer

241 polarimeter. NMR spectral data were obtained with a Bruker Avance-500 spectrometer ($CDCl_3$, δ_H 7.26/δ_C 77.2). HR-TOF-MS data were measured using an Agilent Accurate-Mass-Q-TOF LC/MS 6520 instrument. The purity of synthetic compounds was determined by HPLC, and the compounds with purity of > 95% were used for the following experiments.

Synthesis of 3a-3l, and 3n. The solution of benzaldehyde analogues (**1a-1l,** and **1n**) (10 mmol) in THF (10 mL) and 30 mL of allyl magnesium bromide (1.0 M in THF) were stirred at -78 ºC for 1 h. The reaction was quenched by the addition of $NaHCO_3$ in saturated aqueous solution, followed by 15 min of agitation. The mixture was then concentrated and filtered through a silica plug (~100 g) with hexane/EtOAc (20:1, 1000 mL) as the eluant. The filtrate was concentrated in vacuo to give **2a-2l,** and **2n**

To a solution of alcohols (**2a-2l,** and **2n**) (7.8 mmol) in hexane (10 mL) was added activated MnO_2 (7.2 g, 81 mmol). The solution was stirred for 6 h at room temperature. The resulting mixture was filtered through a pad of celite, and the filtrate was concentrated. The solvent was removed in vacuo to afford crude aldehyde. (*R*)-CBS catalyst (1.0 mol/L, 8.1 mL, 8.1 mmol) and $BH{\cdot}Sme_2$ (10 mol/L, 8.1 mL, 81 mmol) were added into 10 mL of anhydrous CH_2Cl_2 at 20 °C. After stirring for 20 min at 20 °C, the crude aldhyde in anhydrous CH_2Cl_2 (5 mL) was added dropwisely. After 3 h, the reaction was quenched by methanol (10 mL). The resulting mixture was then concentrated and filtered through a silica plug (~100 g) with hexane/EtOAc (20:1, 1000 mL) as the eluant. The filtrate was concentrated in vacuo to give **3a-3l,** and **3n.**

1-phenylprop-2-en-1-ol (2a): colourless oil; UV (methanol) λ_{max} (log ε) 218 (3.20), 249 (0.59) nm; IR (neat) ν_{max} 2810, 1640, 1428, 1423, 1325, 1223, 1018, and 625 cm^{-1}; positive HRTOFMS *m/z* $[M+H]^+$ 135.0810 (calcd. for $C_9H_{11}O$, 135.0810). ^1H NMR data are in accordance with literature data. [44]

1-(2-nitrophenyl)prop-2-en-1-ol (2b): colourless oil; UV (methanol) λ_{max} (log ε) 220 (3.25), 260 (0.50) nm; IR (neat) ν_{max} 2824, 1645, 1425, 1348, 1225, 1029, 798, and 613 cm^{-1}; positive HRTOFMS *m/z* $[M+H]^+$ 180.0655 (calcd. for $C_9H_{10}NO_3$, 180.0655). ^1H NMR data are in accordance with literature data. [45]

1-(p-tolyl)prop-2-en-1-ol (2c): colourless oil; UV (methanol) λ_{max} (log ε) 218 (3.25), 237 (0.34) nm; IR (neat) ν_{max} 2810, 1645, 1623, 1423, 1418, 1225, 1025, 798, 723 cm^{-1}; positive HRTOFMS *m/z* $[M+H]^+$ 149.0970 (calcd. for $C_{10}H_{13}O$, 149.0967). ^1H NMR data are in accordance with literature data. [46]

1-(4-(tert-butyl)phenyl)prop-2-en-1-ol (2d): colourless oil; UV (methanol) λ_{max} (log ε) 220 (3.25), 260 (0.50) nm; IR (neat) ν_{max} 3335, 2810, 2795, 1645, 1620, 1425, 1348, 1253, 1029, 799, 723, and 613 cm^{-1}; positive HRTOFMS *m/z* $[M+H]^+$ 191.1432 (calcd. for $C_{13}H_{19}O$, 191.1430). ^1H NMR (500 MHz, $CDCl_3$): δ 7.38 (d, J = 8.1 Hz, 2H), 7.29 (d, J = 8.1 Hz, 2H), 6.04 (ddd, J = 16.6, 10.3, 10.3 Hz, 1H), 5.34 (d, J = 16.6 Hz, 1H), 5.17 (m, 1H), 1.31 (s, 9H); ^{13}C NMR (125 MHz, $CDCl_3$): δ 150.8, 140.3, 139.7, 126.1 (×2), 125.5 (×2), 114.9, 75.2, 34.6, 31.4 (×3).

1-(4-isopropylphenyl)prop-2-en-1-ol (2e): colourless oil; UV (methanol) λ_{max} (log ε) 218 (3.18), 251 (0.89) nm; IR (neat) ν_{max} 3318, 3152, 2823, 1629, 1442, 1425,

1289, 1225, 925, and 623 cm^{-1}; positive HRTOFMS *m/z* $[M+H]^+$ 177.1280 (calcd. for $C_{12}H_{17}O$, 177.1279). ^1H NMR data are in accordance with literature data. [47]

1-(4-ethylphenyl)prop-2-en-1-ol (2f): colourless oil; UV (methanol) λ_{max} (log ε) 218 (2.85), 260 (0.52) nm; IR (neat) ν_{max} 2823, 2772, 1634, 1608, 1425, 1225, 1025, 795, 723, and 613 cm^{-1}; positive HRTOFMS *m/z* $[M+H]^+$ 163.1118 (calcd. for $C_{11}H_{15}O$, 163.1117). ^1H NMR data are in accordance with literature data. [48]

1-(4-methoxyphenyl)prop-2-en-1-ol (2g): colourless oil; UV (methanol) λ_{max} (log ε) 220 (2.54), 268 (0.78) nm; IR (neat) ν_{max} 3320, 2925, 1625, 1428, 1423, 1245, 1223, 725, and 625 cm^{-1}; positive HRTOFMS *m/z* $[M+H]^+$ 165.0918 (calcd. for $C_{10}H_{13}O_2$, 165.0916). ^1H NMR data are in accordance with literature data. [46]

1-(4-nitrophenyl)prop-2-en-1-ol (2h): colourless oil; UV (methanol) λ_{max} (log ε) 220 (3.23), 237 (0.34) nm; IR (neat) ν_{max} 2825, 1645, 1623, 1452,1423, 1223, 798, 723, 623 cm^{-1}; positive HRTOFMS *m/z* $[M+H]^+$ 149.0965 (calcd. for $C_{10}H_{13}O$, 149.0967). ^1H NMR data are in accordance with literature data. [49]

1-(2,5-difluorophenyl)prop-2-en-1-ol (2i): colourless oil; UV (methanol) λ_{max} (log ε) 220 (3.25), 246 (0.58) nm; IR (neat) ν_{max} 3309, 3128, 2825, 1625, 1445, 1423, 1245, 723, and 618 cm^{-1}; positive HRTOFMS *m/z* $[M+H]^+$ 171.0621 (calcd. for $C_9H_9F_2O$, 171.0621). ^1H NMR data are in accordance with literature data. [50]

1-(3,4,5-trifluorophenyl)prop-2-en-1-ol (2j): colourless oil; UV (methanol) λ_{max} (log ε) 215 (3.23), 268 (0.34) nm; IR (neat) ν_{max} 2895, 2765, 1623, 1608, 1423, 1225, 1125, 798, 623 cm^{-1}; positive HRTOFMS *m/z* $[M+H]^+$ 189.0444 (calcd. for $C_9H_8F_3O$, 189.0444). ^1H NMR (500 MHz, $CDCl_3$): δ 7.00 (d, J = 8.1 Hz, 2H), 5.92 (ddd, J =

17.2, 10.2, 6.5 Hz, 1H), 5.35 (d, J = 17.1 Hz, 1H), 5.25 (d, J = 17.1 Hz, 1H), 5.12 (d, J = 6.5 Hz, 1H); ^{13}C NMR (125 MHz, $CDCl_3$): δ 139.0 (×2), 116.8 (×2), 110.3, 110.3, 110.2, 110.1, 74.0.

1-(2,5-dimethoxyphenyl)prop-2-en-1-ol (2k): colourless oil; UV (methanol) λ_{max} (log ε) 221 (1.25), 254 (2.59) nm; IR (neat) ν_{max} 3316, 2825, 2421, 1640, 1445, 1428, 1327, 1245, 1228, 928, and 625 cm^{-1}; positive HRTOFMS *m/z* $[M+H]^+$ 195.1022 (calcd. for $C_{11}H_{15}O_3$, 195.1021). ^{1}H NMR data are in accordance with literature data.[49]

1-(2-(methoxymethoxy)phenyl)prop-2-en-1-ol (2l): colourless oil; UV (methanol) λ_{max} (log ε) 218 (1.25), 287 (2.59), 311 (1.32) nm; IR (neat) ν_{max} 3321, 1655, 1442, 1428, 1321, 1212, 723, and 625 cm^{-1}; positive HRTOFMS *m/z* $[M+H]^+$ 195.1025 (calcd. for $C_{11}H_{15}O_3$, 195.1021). ^{1}H NMR data are in accordance with literature data. [51]

1-(naphthalen-2-yl)prop-2-en-1-ol (2n): yellow oil; UV (methanol) λ_{max} (log ε) 218 (2.28), 272 (1.58), 321 (1.98) nm; IR (neat) ν_{max} 3310, 3115, 2823, 1643, 1476, 1445, 1425, 1423, 1245, 1223, 723, and 625 cm^{-1}; positive HRTOFMS *m/z* $[M+H]^+$ 185.0966 (calcd. for $C_{13}H_{13}O$, 185.0966). ^{1}H NMR data are in accordance with literature data. [51]

(*R*)-1-phenylprop-2-en-1-ol (3a): colourless oil; $[\alpha]^{25}_D$ +16.0 (c 0.1 mg/mL, MeOH); the IR and ^{1}H and ^{13}C NMR data of **3a** are those of **2a**; positive HRTOFMS *m/z* $[M+H]^+$ 135.0812 (calcd. for $C_9H_{11}O$, 135.0810).

(*R*)-1-(2-nitrophenyl)prop-2-en-1-ol (3b): colourless oil; $[\alpha]^{25}_{D}$ +49.0 (c 0.1 mg/mL, MeOH); the IR and ^{1}H and ^{13}C NMR data of **3b** are identical with those of **2b**; positive HRTOFMS *m/z* $[M+H]^{+}$ 180.0655 (calcd. for $C_9H_{10}NO_3$, 180.0655).

(*R*)-1-(p-tolyl)prop-2-en-1-ol (3c): colourless oil; $[\alpha]^{25}_{D}$ +25.0 (c 0.1 mg/mL, MeOH); the IR and ^{1}H and ^{13}C NMR data of **3c** are identical with those of **2c**; positive HRTOFMS *m/z* $[M+H]^{+}$ 149.0966 (calcd. for $C_{10}H_{13}O$, 149.0967).

(*R*)-1-(4-(tert-butyl)phenyl)prop-2-en-1-ol (3d): colourless oil; $[\alpha]^{25}_{D}$ +54.2 (c 0.1 mg/mL, MeOH); the IR and ^{1}H and ^{13}C NMR data of **3d** are identical with those of **2d**; positive HRTOFMS *m/z* $[M+H]^{+}$ 191.1432 (calcd. for $C_{13}H_{19}O$, 191.1430).

(*R*)-1-(4-isopropylphenyl)prop-2-en-1-ol (3e): colourless oil; $[\alpha]^{25}_{D}$ +89.0 (c 0.1 mg/mL, MeOH); the IR and ^{1}H and ^{13}C NMR data of **3e** are identical with those of **2e**; positive HRTOFMS *m/z* $[M+H]^{+}$ 177.1279 (calcd. for $C_{12}H_{17}O$, 177.1279).

(*R*)-1-(4-ethylphenyl)prop-2-en-1-ol (3f): colourless oil; $[\alpha]^{25}_{D}$ +32.0 (*c* 0.1 mg/mL, MeOH); the IR and ^{1}H and ^{13}C NMR data of **3f** are identical with those of **2f**; positive HRTOFMS *m/z* $[M+H]^{+}$ 163.1118 (calcd. for $C_{11}H_{15}O$, 163.1117).

(*R*)-1-(4-methoxyphenyl)prop-2-en-1-ol (3g): colourless oil; $[\alpha]^{25}_{D}$ +23.0 (*c* 0.1 mg/mL, MeOH); the IR and ^{1}H and ^{13}C NMR data of **3g** are identical with those of **2g**; positive HRTOFMS *m/z* $[M+H]^{+}$ 165.0916 (calcd. for $C_{10}H_{13}O_2$, 165.0916).

(*R*)-1-(4-nitrophenyl)prop-2-en-1-ol (3h): colourless oil; $[\alpha]^{25}_{D}$ +9.0 (c 0.1 mg/mL, MeOH); the IR and ^{1}H and ^{13}C NMR data of **3h** are identical with those of **2h**; positive HRTOFMS *m/z* $[M+H]^{+}$ 180.0655 (calcd. for $C_9H_{10}NO_3$, 180.0655).

(*R*)-1-(2,5-difluorophenyl)prop-2-en-1-ol (3i): colourless oil; $[\alpha]^{25}_{D}$ +25.0 (c 0.1 mg/mL, MeOH); the IR and ^{1}H and ^{13}C NMR data of **3i** are identical with those of **2i**; positive HRTOFMS *m/z* $[M+H]^{+}$ 171.0625 (calcd. for $C_9H_8F_2O$, 171.0621).

(*R*)-1-(3,4,5-trifluorophenyl)prop-2-en-1-ol (3j): colourless oil; $[\alpha]^{25}_{D}$ +23.1 (c 0.1 mg/mL, MeOH); the IR and ^{1}H and ^{13}C NMR data of **3j** are identical with those of **2j**; positive HRTOFMS *m/z* $[M+H]^{+}$ 189.0448 (calcd. for $C_9H_7F_3O_3$, 189.0444).

(*R*)-1-(2,5-dimethoxyphenyl)prop-2-en-1-ol (3k): colourless oil; $[\alpha]^{25}_{D}$ +42.0 (c 0.1 mg/mL, MeOH); the IR and ^{1}H and ^{13}C NMR data of **3k** are identical with those of **2l**; positive HRTOFMS *m/z* $[M+H]^{+}$ 195.1021 (calcd. for $C_{11}H_{15}O_3$, 195.1021).

(*R*)-1-(2-(methoxymethoxy)phenyl)prop-2-en-1-ol (3l): colourless oil; $[\alpha]^{25}_{D}$ +39.0 (c 0.1 mg/mL, MeOH); the IR and ^{1}H and ^{13}C NMR data of **3l** are identical with those of **2l**; positive HRTOFMS *m/z* $[M+H]^{+}$ 195.1020 (calcd. for $C_{11}H_{15}O_3$, 195.1021).

(*R*)-1-(naphthalen-2-yl)prop-2-en-1-ol (3n): yellow oil; $[\alpha]^{25}_{D}$ +8.0 (c 0.1 mg/mL, MeOH); the IR and ^{1}H and ^{13}C NMR data of **3n** are identical with those of **2n**; positive HRTOFMS *m/z* $[M+H]^{+}$ 185.0968 (calcd. for $C_{13}H_{13}O$, 185.0966).

Synthesis of (*E*)-7,11-dimethyl-3-methylenedodeca-6,10-dienoic acid (6). With geraniol as starting material, compound **6** (3.16 g, 85%) was obtained via **5** (6.07 g, 90% yield) as an intermediate according to the previously reported method.[25]

Compound 6: colorless oil; ^{1}H NMR (500 MHz, $CDCl_3$): δ 6.29 (s, 1H), 5.65 (s, 1H), 5.09 (m, 2H), 2.35 (t, J = 7.8 Hz, 2H), 2.16 (t, J = 7.8, 2H), 2.06 (t, J = 7.8 Hz, 2H), 1.98 (t, J = 7.8 Hz, 2H), 1.78 (s, 3H), 1.60 (s, 6H); IR (neat) ν_{max} 3212, 2945,

2915, 1694, 1635, 1425, 1304, 942 cm^{-1}; positive HRTOFMS *m/z* $[M+H]^+$ 223.1692 (calcd. for $C_{14}H_{23}O_2$, 223.1693).

Synthesis of 7a-7n. By the same method as described for ganomycin I, compounds **3a-3m** were connected, and further converted into analogues **7a-7n**.

(*R*,*E*)-3-(4,8-dimethylnona-3,7-dien-1-yl)-5-phenylfuran-2(5H)-one (7a): Colorless oil; $[\alpha]^{25}_D$ + 16.0 (c 0.1 mg/mL, MeOH); IR (neat) ν_{max} 3210, 2873, 1662, 1632, 1445, 1423, 1237, 942, 712, 623 cm^{-1}; positive HRTOFMS *m/z* $[M+H]^+$ 311.2012 (calcd. for $C_{21}H_{27}O_2$, 311.2011). ^{1}H NMR (500 MHz, $CDCl_3$): δ 7.37 (d, J = 7.1 Hz, 2H), 7.25 (m, 3H) 7.08 (s, 1H), 5.87 (s, 1H), 5.12 (d, J = 7.5 Hz, 1H), 5.07 (d, J = 7.5 Hz, 1H), 2.41 (t, J= 7.8 Hz, 2H), 2.32 (t, J=7.8 Hz, 2H), 2.05 (t, J = 7.8 Hz, 2H), 1.98 (t, J = 7.8 Hz, 2H), 1.67 (s, 3H), 1.59 (s, 6H); ^{13}C NMR (125 MHz, $CDCl_3$): δ 173.9, 147.9, 136.9, 135.2, 133.5, 131.5, 129.1, 128.9 (×2), 126.5 (×2), 124.1, 122.6, 82.3, 39.6, 26.6, 25.7 (×2), 25.4, 17.7, 16.2.

(*R*,*E*)-3-(4,8-dimethylnona-3,7-dien-1-yl)-5-(2-nitrophenyl)furan-2(5H)-one (7b): Colorless oil; $[\alpha]^{25}_D$ + 38.0 (c 0.1 mg/mL, MeOH); IR (neat) ν_{max} 2932, 1693, 1654, 1423, 1418, 1265, 1245, 942, 712 cm^{-1}; positive HRTOFMS *m/z* $[M+H]^+$ 356.1856 (calcd. for $C_{21}H_{26}NO_4$, 356.1856). ^{1}H NMR (500 MHz, $CDCl_3$): δ 8.17 (d, J = 8.1 Hz, 1H), 7.68 (t, J = 7.6 Hz) 7.53 (t, J = 8.1 Hz, 2H), 7.34 (s, 1H), 6.53 (s, 1H), 5.06 (m, 2H), 2.38 (t, J = 7.8 Hz, 2H), 2.27 (t, J =7.8 Hz, 2H), 1.99 (t, J = 7.8 Hz, 2H), 1.94 (t, J = 7.8 Hz, 2H), 1.66 (s, 3H), 1.57 (s, 3H), 1.56 (s, 3H); ^{13}C NMR (125 MHz, $CDCl_3$): δ 173.7, 148.1, 147.9, 137.0, 134.7, 133.6, 132.3, 131.5, 129.4, 126.8 125.3, 124.1, 122.3, 78.4, 39.6, 26.6, 25.7 (×2), 25.4, 17.7, 16.1.

(*R*,*E*)-3-(4,8-dimethylnona-3,7-dien-1-yl)-5-(p-tolyl)furan-2(5H)-one (7c): Colorless oil; $[\alpha]^{25}_{D}$ + 21.0 (c 0.1 mg/mL, MeOH); IR (neat) ν_{max} 2893, 2877, 1654, 1625, 1425, 1398, 1344, 1223, 945, 723 cm^{-1}; positive HRTOFMS *m/z* $[M+H]^+$ 325.2164 (calcd. for $C_{22}H_{29}O_2$, 325.2162). ^1H NMR (500 MHz, $CDCl_3$): δ 7.18 (d, *J* = 8.1 Hz, 2H), 7.13 (d, *J* = 8.1 Hz, 2H), 7.05 (s, 1H), 5.83 (s, 1H), 5.12 (t, *J* = 7.2 Hz, 1H), 5.07 (t, *J* = 7.2 Hz, 1H), 2.40 (t, *J* = 7.8 Hz, 2H), 2.35 (s, 3H), 2.31 (t, *J* = 7.8 Hz, 2H), 2.04 (t, *J* = 7.8 Hz, 2H), 1.99 (t, *J* =7.8 Hz, 2H), 1.67 (s, 3H), 1.59 (s, 6H); ^{13}C NMR (125 MHz, $CDCl_3$): δ 174.0, 147.9, 139.1, 136.8, 133.5, 132.1, 131.5, 129.8 (×2), 126.6 (×2), 124.1, 122.6, 82.2, 39.6, 26.6, 25.7, 25.7, 25.4, 21.2, 17.7, 16.2.

(*R*,*E*)-5-(4-(tert-butyl)phenyl)-3-(4,8-dimethylnona-3,7-dien-1-yl)furan-2(5H)-one (7d): Colorless oil; $[\alpha]^{25}_{D}$ + 58.0 (c 0.1 mg/mL, MeOH); IR (neat) ν_{max} 3212, 2923, 2907, 1694, 1631, 1423, 1418, 1304, 1245, 942, 725 cm^{-1}; positive HRTOFMS *m/z* $[M+H]^+$ 367.2632 (calcd. for $C_{25}H_{35}O_2$, 367.2632). ^1H NMR (500 MHz, $CDCl_3$): δ 7.40 (d, *J* = 8.1 Hz, 2H), 7.18 (d, *J* = 8.1 Hz, 2H), 7.06 (d, *J* = 11.9 Hz, 1H), 5.85 (s, 1H), 5.12 (t, *J* = 6.5 Hz, 1H), 5.07 (t, *J* = 6.5 Hz, 1H), 2.40 (t, *J* = 7.8 Hz, 2H), 2.31 (t, *J* = 7.8 Hz, 2H), 2.05 (t, *J* = 7.8 Hz, 2H), 1.98 (t, *J* = 7.8 Hz, 2H), 1.67 (s, 3H), 1.59 (s, 6H), 1.31 (s, 9H); ^{13}C NMR (125 MHz, $CDCl_3$): δ 174.0, 152.3, 147.9, 136.8, 133.5, 132.1, 131.5, 126.4 (×2), 125.9 (×2), 124.1, 122.6, 82.2, 39.6, 34.7, 31.2 (×3), 26.6, 25.7, 25.7, 25.4, 17.7, 16.2.

(*R*,*E*)-3-(4,8-dimethylnona-3,7-dien-1-yl)-5-(4-isopropylphenyl)furan-2(5H)-one (7e): Colorless oil; $[\alpha]^{25}_{D}$ + 48.0 (c 0.1 mg/mL, MeOH); IR (neat) ν_{max} 3312, 2828, 1645, 1623, 1465, 1425, 1371, 1225, 723, 623 cm^{-1}; positive HRTOFMS *m/z* $[M+H]^+$

353.2481 (calcd. for $C_{24}H_{33}O_2$, 353.2481). ^{1}H NMR (500 MHz, Acetone-d_6): δ 7.36 (s, 1H), 7.30 (d, J = 7.5 Hz, 2H), 7.24 (d, J = 7.5 Hz, 2H), 5.89 (s, 1H), 5.19(d, J = 7.5 Hz, 1H), 5.06 (d, J = 7.5 Hz, 1H), 2.92 (m, 1H), 2.36 (m, 4H), 2.09 (t, J = 7.8 Hz, 2H), 2.00 (t, J = 7.8 Hz, 2H), 1.65 (s, 3H), 1.62 (s, 3H), 1.59 (s, 3H), 1.24 (d, J = 7.5 Hz, 6H).

(*R*,*E*)-3-(4,8-dimethylnona-3,7-dien-1-yl)-5-(4-ethylphenyl)furan-2(5H)-one (7f): Colorless oil; $[\alpha]^{25}_D$ + 54.0 (c 0.1 mg/mL, MeOH); IR (neat) ν_{max} 2925, 2918, 1652, 1624, 1424, 1303, 1223, 923, 723 cm^{-1}; positive HRTOFMS *m/z* $[M+H]^+$ 339.2320 (calcd. for $C_{23}H_{31}O_2$, 339.2319). ^{1}H NMR (500 MHz, $CDCl_3$): δ 7.20 (d, J = 8.1 Hz, 2H), 7.16 (d, J = 8.1 Hz, 2H), 7.06 (s, 1H), 5.84 (s, 1H), 5.12 (t, J = 6.5 Hz, 1H), 5.07 (t, J= 6.5 Hz, 1H), 2.65 (q, J = 7.6 Hz, 2H), 2.41 (t, J = 7.8 Hz, 2H), 2.31 (t, J = 7.8 Hz, 2H), 2.04 (t, J = 7.8 Hz, 2H), 1.98 (t, J = 7.8 Hz, 2H), 1.67 (s, 3H), 1.59 (s, 6H), 1.23 (t, J = 7.6 Hz, 3H); ^{13}C NMR (125 MHz, $CDCl_3$): δ 174.0, 147.9, 145.4, 136.8, 133.5, 132.4, 131.5, 128.4 (×2), 126.6 (×2), 124.1, 122.6, 82.3, 39.6, 28.6, 26.6, 25.7, 25.7, 25.4, 17.7, 16.2, 15.5.

(*R*,*E*)-3-(4,8-dimethylnona-3,7-dien-1-yl)-5-(4-methoxyphenyl)furan-2(5H)-one (7g): Colorless oil; $[\alpha]^{25}_D$ + 78.0 (c 0.1 mg/mL, MeOH); IR (neat) ν_{max} 3310, 2723, 1665, 1446, 1422, 1225, 823, 723, 625 cm^{-1}; positive HRTOFMS *m/z* $[M+H]^+$ 341.2120 (calcd. for $C_{22}H_{28}O_3$, 341.2117). ^{1}H NMR (500 MHz, $CDCl_3$): δ 7.13 (t, J = 7.7 Hz, 2H), 7.07(d, J = 7.5 Hz, 2H), 6.81 (d, J = 7.7 Hz, 1H), 6.15(d, J = 7.5 Hz, 1H), 5.03(d, J = 7.5 Hz, 1H), 4.99(d, J = 7.5 Hz, 1H), 3.42 (s, 3H), 2.38 (t, J = 7.8 Hz, 2H), 2.28 (t, J = 7.8 Hz, 2H), 2.02 (t, J = 7.8 Hz, 2H), 1.96 (t, J = 7.8 Hz, 2H), 1.67 (s, 3H),

1.59 (s, 3H), 1.58 (s, 3H); ^{13}C NMR (125 MHz, $CDCl_3$): δ 174.2, 153.1, 147.8, 136.9, 133.2, 131.6, 129.9, 126.6, 124.2, 122.7, 122.2, 121.2, 115.8, 78.1, 51.0, 39.6, 26.6, 25.7 (×2), 25.4, 17.7, 16.1.

(*R*,*E*)-3-(4,8-dimethylnona-3,7-dien-1-yl)-5-(4-nitrophenyl)furan-2(5H)-one (7h): Colorless oil; $[\alpha]^{25}_D$ + 92.0 (c 0.1 mg/mL, MeOH); IR (neat) ν_{max} 2932, 1692, 1648, 1425, 1418, 1248, 1225, 845, 725, 623 cm^{-1}; positive HRTOFMS *m/z* $[M+H]^+$ 356.1856 (calcd. for $C_{21}H_{26}NO_4$, 356.1856). ^{1}H NMR (500 MHz, $CDCl_3$): δ 8.07 (d, *J* = 7.4 Hz, 2H), 7.48 (d, *J* = 7.4 Hz, 2H) 7.29 (m, 2H), 7.34 (s, 1H), 5.01 (t, *J* = 7.4 Hz, 1H), 4.98 (t, *J* = 7.4 Hz, 1H), 2.34 (t, *J* = 7.8 Hz, 2H), 2.19 (t, *J* = 7.8 Hz, 2H), 1.92 (t, *J* = 7.8 Hz, 2H), 1.88 (t, *J* = 7.8 Hz, 2H), 1.67 (s, 3H), 1.57 (s, 6H).

(*R*,*E*)-5-(2,5-difluorophenyl)-3-(4,8-dimethylnona-3,7-dien-1-yl)furan-2(5H)-one (7i): Colorless oil; $[\alpha]^{25}_D$ + 89.0 (c 0.1 mg/mL, MeOH); IR (neat) ν_{max} 2893, 1623, 1448, 1422, 1252, 1224, 842, 723, 625 cm^{-1}; positive HRTOFMS *m/z* $[M+H]^+$ 347.1823 (calcd. for $C_{21}H_{24}F_2O_2$, 347.1823). ^{1}H NMR (500 MHz, $CDCl_3$): δ 7.33 (m, 1H), 7.07 (s, 1H), 6.90 (t, *J* = 7.4 Hz, 2H), 6.22 (s, 1H), 5.13 (t, *J* = 7.4 Hz, 1H), 5.07 (t, *J* = 7.4 Hz, 1H), 2.42 (t, *J* = 7.8 Hz, 2H), 2.32 (t, *J* =7.8 Hz, 2H), 2.05 (t, *J* = 7.8 Hz, 2H), 1.99 (t, *J* = 7.8 Hz, 2H), 1.66 (s, 3H), 1.61 (s, 3H), 1.59 (s, 3H).

(*R*,*E*)-3-(4,8-dimethylnona-3,7-dien-1-yl)-5-(3,4,5-trifluorophenyl)furan-2(5H)-one (7j): Colorless oil; $[\alpha]^{25}_D$ + 21.0 (c 0.1 mg/mL, MeOH); IR (neat) ν_{max} 2923, 2907, 1694, 1625, 1423, 926, 723 cm^{-1}; ^{1}H NMR (500 MHz, $CDCl_3$): δ 7.02 (d, *J* = 8.1 Hz, 1H), 6.91 (t, *J* = 8.1 Hz, 2H), 5.77 (s, 1H), 5.08 (m, 2H), 2.41 (t, *J* = 7.8 Hz, 2H), 2.31 (t, *J* = 7.8 Hz, 2H), 2.03 (t, *J* = 7.8 Hz, 2H), 1.98 (t, *J* = 7.8 Hz, 2H), 1.67 (s,

3H), 1.59 (s, 6H); ^{13}C NMR (125 MHz, $CDCl_3$): δ 172.9, 146.4, 137.2, 134.6, 131.6, 124.0 (×2), 122.3 (×2), 110.9, 110.8, 110.7, 110.7, 80.2, 39.6, 26.6, 25.7, 25.6, 25.4, 17.7, 16.2; positive HRTOFMS *m/z* $[M+H]^+$ 365.1726 (calcd. for $C_{21}H_{24}F_3O_2$, 365.1723).

(R,E)-5-(2,5-dimethoxyphenyl)-3-(4,8-dimethylnona-3,7-dien-1-yl)furan-2(5H)-one (7k): Colorless oil; $[\alpha]^{25}_D$ + 44.2 (c 0.1 mg/mL, MeOH); IR (neat) ν_{max} 3303, 2901, 1723, 1623, 1444, 1421, 1225, 825, 729, 627 cm^{-1}; positive HRTOFMS *m/z* $[M+H]^+$ 371.2193 (calcd. for $C_{23}H_{31}O_4$, 371.2196). ^{1}H NMR (500 MHz, $CDCl_3$): δ 7.19 (s), 6.83 (m, 2H) 6.76 (m, 1H), 6.19 (m, 1H), 5.11 (d, *J* = 7.5 Hz, 1H), 5.07 (d, *J* = 7.5 Hz, 1H), 3.84 (s, 3H), 3.74 (s, 3H), 2.35 (t, *J* = 7.8 Hz, 2H), 2.27 (t, *J* = 7.8 Hz, 2H), 2.01 (t, *J* = 7.8 Hz, 2H), 1.95 (t, *J* = 7.8 Hz, 2H), 1.67 (s, 3H), 1.58 (s, 6H);

(*R,E*)-3-(4,8-dimethylnona-3,7-dien-1-yl)-5-(2-(methoxymethoxy)phenyl)furan-2(5H)-one (7l): Colorless oil; $[\alpha]^{25}_D$ + 71.0 (c 0.1 mg/mL, MeOH); IR (neat) ν_{max} 3310, 2912, 1701, 1645, 1452, 1445, 1423, 1225, 823, 734, 625 cm^{-1}; positive HRTOFMS *m/z* $[M+H]^+$ 371.2196 (calcd. for $C_{23}H_{31}O_4$, 371.2196). ^{1}H NMR (500 MHz, $CDCl_3$): δ 7.28 (dd, *J* = 7.1, 2.5 Hz, 1H), 7.18 (m, 1H) 7.08 (m, 2H), 7.01 (m, 1H), 6.26 (d, *J* = 7.5 Hz, 1H), 5.30 (s, 2H), 5.11 (d, *J* = 7.5 Hz, 1H), 5.07 (d, *J* = 7.5 Hz, 1H), 3.51 (s, 2H), 2.37 (t, *J* = 7.8 Hz, 2H), 2.28 (t, *J* = 7.8 Hz, 2H), 2.02 (t, *J* = 7.8 Hz, 2H), 1.96 (t, *J* = 7.8 Hz, 2H), 1.67 (s, 3H), 1.58 (s, 6H);

(*R,E*)-3-(4,8-dimethylnona-3,7-dien-1-yl)-5-(2-hydroxyphenyl)furan-2(5H)-one (7m): Colorless oil; $[\alpha]^{25}_D$ + 54.0 (c 0.1 mg/mL, MeOH); IR (neat) ν_{max} 3325, 3310, 2923, 1628, 1455, 1423, 1223, 725, 623 cm^{-1}; positive HRTOFMS *m/z* $[M+H]^+$

327.1883 (calcd. for $C_{21}H_{27}O_3$, 327.1882). ^{1}H NMR (500 MHz, $CDCl_3$): δ 7.21 (t, J = 7.7, 2H), 7.15 (d, J = 7.5, 1H), 6.93 (t, J = 7.5, 1H), 6.81 (d, J = 7.7, 1H), 6.23 (d, J = 7.5 Hz, 1H), 5.11 (d, J = 7.5 Hz, 1H), 5.06(d, J = 7.5 Hz, 1H), 2.38 (t, J = 7.8 Hz, 2H), 2.29 (t, J = 7.8 Hz, 2H), 2.02 (t, J = 7.8 Hz, 2H), 1.96 (t, J =7.8 Hz, 2H), 1.67 (s, 3H), 1.59 (s, 3H), 1.58 (s, 3H); ^{13}C NMR (125 MHz, $CDCl_3$): δ 174.1, 153.0, 147.7, 136.8, 133.1, 131.5, 129.8, 126.6, 124.2, 122.6, 122.1, 121.3, 115.8, 78.0, 39.6, 26.6, 25.7 (×2), 25.4, 17.7, 16.1.

(*R*,*E*)-3-(4,8-dimethylnona-3,7-dien-1-yl)-5-(naphthalen-2-yl)furan-2(5H)-one (7n): Colorless oil; $[\alpha]^{25}_D$ + 17.0 (c 0.1 mg/mL, MeOH); IR (neat) ν_{max} 3121, 1643, 1624, 1465, 1445,1425, 1227, 825, 725, 623 cm^{-1}; positive HRTOFMS *m/z* $[M+H]^+$ 361.2171 (calcd. for $C_{25}H_{28}O_2$, 361.2168). ^{1}H NMR (500 MHz, $CDCl_3$): δ 8.08 (d, J = 8.4 Hz, 1H), 7.91 (d, J = 8.4 Hz, 1H), 7.86 (d, J = 8.4 Hz, 1H), 7.60 (t, J = 7.4 Hz, 1H), 7.56 (t, J = 7.4 Hz, 1H), 7.44 (m, 1H), 7.37 (m, 2H), 6.66 (s, 1H), 5.13 (t, J = 7.4 Hz, 1H), 5.06 (t, J = 7.4 Hz, 1H), 2.43 (t, J= 7.8 Hz, 2H), 2.33 (t, J=7.8 Hz, 2H), 2.02 (t, J = 7.8 Hz, 2H), 1.97 (t, J =7.8 Hz, 2H), 1.66 (s, 3H), 1.59 (s, 3H), 1.58 (s, 3H); ^{13}C NMR (125 MHz, $CDCl_3$): δ 173.8, 147.4, 136.9, 134.0, 133.8, 131.5, 131.3, 130.7, 129.6, 129.1, 126.9, 126.1, 125.4, 124.1, 123.5, 122.6, 122.5, 79.3, 39.6, 26.6, 25.7 (×2), 25.5, 17.7, 16.2.

Inhibition Assay against *α*-Glucosidase and HMG-CoA Reductase. The preperation of ***α***-glucosidase from rat small intestinal mucosa and HMG-CoA reductase from pig liver was performed as previously described.[24] The bioassay was conducted using a 96-well plate, and the absorbance was determined at 405 nm using

a Spectra Max 190 microplate reader (Molecular Devices Inc.). The enzyme assay were performed in triplicate with different concentrations of individual compounds. Each concentration was repeated three times in parallel. The control was prepared by adding a phosphate buffer instead of tested compounds. The blank was prepared by adding phosphate buffer instead of the α-glucosidase or HMG-CoA reductase. The inhibition rates (%) = [(OD $_{control}$ - OD $_{control\ blank}$)-(OD $_{test}$-OD $_{test\ blank}$)]/ (OD $_{control}$ - OD $_{control\ blank}$) × 100%.

In an another assay against α-glucosidase, the enzyme reaction product (4-nitrophenol) was immediately dectected after incubation by a HPLC method. Each concentration was repeated 3 times in parallel. The gradient elution started with 20% acetonitrile in water (with 0.1 ‰ trifluoroacetic acid) and linearly increased to 100% acetonitrile in 10 min, and followed by 5 min of re-equilibration. The inhibition rates (%) =[(Area $_{control}$ - Area $_{control\ blank}$)-Area $_{test}$]/ (Area $_{control}$ - Area $_{control\ blank}$) × 100%. IC_{50} values were determined by the inhibition rates of different concentration gradients and calculated by Graphpad 6.0.

Animal care and experiments. All procedures were performed in accordance with recommendations in the Guide for the Care and Use of Laboratory Animals of the Institute of Microbiology, Chinese Academy of Sciences (IMCAS) Ethics Committee. The protocol was approved by the Committee on the Ethics of Animal Experiments of IMCAS (permit no. APIMCAS2017023). C57BL/*6J* and *ob/ob* mice were purchased from the Experimental Animal Center, Chinese Academy of Medical Sciences. For Abx mice study, male *ob/ob* mice were fed with ampicillin (1 g/L), vancomycin (0.5

g/L), neomycin (0.5 g/L), gentamycin (100 mg/L), and erythromycin (10 mg/L) in drinking water beginning at 7-8 weeks of age through 10-11 weeks of age.[52] Cecum observation and anaerobic cultivation of faecal samples confirmed successful depletion of gut microbiota after the antibiotic treatment.[53] In the study with DIO mice, the C57BL/*6J* mice were fed with a high-fat diet (60 kcal% fat, 20 kcal% proteins and 20 kcal% carbo-hydrates, Cat. D12492i, Research Diet, New Brun-swick, NJ, USA) at the age of 8 weeks and maintained on the same diet for 8 weeks. Eight-week-old male *ob/ob* mice were kept on normal chow diet (NCD, 13.5 % calories from fat) that was purchased from Vital River Laboratory Animal Technology Co., Ltd. (Beijing, China). Mice were housed in a 12-h dark-light cycle, with the dark cycle encompassing 7 p.m. to 7 a.m., and had free access to food and water.

For the long-term safety assay, 20 male and 20 female C57BL/*6J* mice were sorted into four groups (n = 10 each, two male and two female groups) based on gender, blood glucose level, and body weight. The treatment groups (one male, one female) were given 30.0 mg/kg of **7d** daily by gavage. The vehicle groups (one male, one female) were given oral gavage of an equivalent volume of soybean (Pharmaceutical excipients, Maya Regent, Zhejiang, China). Daily treatment continued for three months. Behavior, survival, body weight, blood glucose, liver function, and organ coefficients were recorded.

In assays with **7d** on male *ob/ob* mice, animals were sorted into six groups (n = 10 each) based on their blood glucose levels and body weight. **7d**-treated groups were

given with **7d** (3.0 mg/kg, 1.0 mg/kg, and 0.3 mg/kg) daily by gavage. Acarbose-treated group was given with acarbose (10.0 mg/kg). The vehicle group was treated with an oral gavage of an equivalent volume of soybean. Treatments continued for 31 days. Body composition was assessed by using 7.5 MHz time domain-nuclear magnetic resonance (TD-NMR; LF50 Minispec, Bruker, Rheinstetten, Germany).

In assays with **7d** on the DIO mice, male C57BL/*6J* mice fed with high-fat diet were sorted into five groups (n = 8 each) based on their blood glucose levels and body weight. Compound **7d** treated groups were daily administrated with **7d** (3.0 mg/kg, 1.0 mg/kg, and 0.3 mg/kg), Ganomycin I-treated group was given with ganomycin I (3.0 mg/kg) daily. Vehicle groups (normal diet and high-fat diet) were treated with an oral gavage of an equivalent volume of soybean. Treatment was continued for 5 weeks.

In the Abx experiments, sixteen male *ob/ob* mice and sixteen Abx male *ob/ob* mice were sorted into five groups (n = 8 each) based on their blood glucose levels and body weight. Treatment group of *ob/ob* mice was given 3.0 mg/kg/day **7d** by mouth. The vehicle group of *ob/ob* mice was given an equivalent volume of soybean by gavage. The treatment group of Abx *ob/ob* mice was given 3.0 mg/kg/day of **7d**, and the vehicle group of Abx *ob/ob* mice was given an equivalent volume of soybean. All treatments continued for 3 weeks.

Tissue sampling. After treatment, animals were anesthetized with diethyl ether (Beijing Chemical Works, Beijing, China) and blood was sampled from the portal and cava veins. After exsanguination, mice were euthanized by cervical dislocation.

Subcutaneous adipose tissue depots, intestines and liver were precisely dissected, weighed, immersed immediately in liquid nitrogen, and stored at −80 °C for further analysis.

PK sample determination by UPLC –MS. For in vivo PK study**,** six healthy male Sprague-Dawley (SD) rats weighing 0.21–0.23 kg were orally administrated with dosage of 2.0 mg/ kg. At 0 (prior to dosing), 0.5, 1, 2, 4, 6, 8, 10, 12, 14, and 16 h after dosing, a blood sample (～200 μL) was collected from each animal via the fosse orbital vein using heparinized 1.5 mL centrifuge tube. Plasma was separated from the blood by centrifugation (4000 rpm for 10 min) and stored at −70℃until analysis.

To 50 μL portion of each plasma sample, 5 μL of internal standard solution (**7f**) was added and vortexed for 1.0 min. Then 100 μL methanol was added for protein precipitation. The mixture was vortexed for 3.0 min followed by centrifugation at 11093 x g for 20 min. 50 μL supernatant was transferred into another clean 1.5 mL centrifuge tube and mixed with 50 μL water. The mixture solution was vortexed for 3.0 min, and a 5 μL aliquot of was injected for the UPLC-MS analysis. Chromatography separation was carried out on an ACQUITY UPLC BEH C18 column (50 mm×2.1 mm i.d., 1.7 μm; Waters Corp., Milford, MA, USA) using an ACQUITY^{TM} UPLC system (Waters Corp., Milford, MA, USA) equipped with a sample manager organizer, an online degasser, a binary solvent management system, and an auto-sampler. Gradient elution was performed with a mixture of methanol (mobile phase A) and water with 0.3 % formic acid (pH 2.5) (mobile phase B) as follows: 0–0.4 min 20% A, 0.4–0.41 min 20–85% A, 0.41–2.0 min 85-95% A, 2.0–

3.0 min 95% A, 3.0–4.0 min 20 % A. The flow rate was kept at a constant 0.4 mL/min and the total run time was 4.0 min. The temperatures of column and auto-sampler were maintained at 40 □ and 4 □, respectively. The sample injection volume was 10 µl. Mass spectrometric detection was performed using a quadrupole-time of flight mass spectrometer equipped with electrospray ionization (ESI) in the positive ionization mode with optimal operation parameters as follows: capillary voltage: 0.5 kV; cone voltage: 35 V; extractor voltage: 4.0 V; source temperature: 110°C; desolvation temperature: 550 °C. The desolvation and cone gas flow rates were 800 L/h and 40 L/h, respectively. Single ion monitoring (SIM) mode was employed for quantification: m/z 367.2637 for **7d** and m/z 339.2324 for **7f** (I.S.), respectively. All data were collected and processed by using MassLynx^{TM} NT 4.1 software with a QuanLynx^{TM} program (Waters Corp., Milford, MA, USA). The linear range of this method was 0.54–107 ng/ml with an *r* (correlation coefficient) value of not less than 0.99.

Biochemical Analysis. Levels of serum glucose, total cholesterol (TC, T-CHO), triglycerides (TG), free fatty acids (FFA), high density lipoprotein cholesterol (HDL-C), low density lipoprotein cholesterol (LDL-C), glycated hemoglobin A1C (HbA1C) and insulin levels were measured as previously described.[24] The insulin sensitivity index (ISI) was calculated from the values of fasting blood glucose (FBG, in mg/dL) and fasting blood insulin (FBI, in mU/L). ISI = 1 / 1000 (FBG×FBI). Hepatic hydroxyproline content after hydrolysis of 300 mg liver samples in 6 N HCl at 110ºC for 16 h was measured as previously described.[20] Serum LPS and TNFα

levels were quantified using LPS and TNFα enzyme-linked immunosorbent assay (ELISA) kit (CUSABIO, Wuhan, China) following the manufacturer's instructions. The level of nitrate in the ileum was determined by the Griess assay as described previously. [42]

Insulin tolerance test (ITT) and oral glucose tolerance test (OGTT). ITT was performed by injecting insulin (0.6 U/kg) intraperitoneally after a 4-hour fasting. OGTT was performed by oral administration of a glucose bolus (2 g/kg) after overnight fasting. The level of blood glucose was measured using a glucose meter (Accu Check, Roche, Switzerland) before oral glucose load (0 min) and at 40, 80, and 120 min after oral glucose load. The area under the curves (AUCs) generated from the data collected during the OGTT was calculated by Graphpad 6.0.

Oral sucrose and maltase tolerance test (OSTT and OMTT). OSTT or OMTT was performed by oral administration of sucrose ormaltose (4.0 g/kg) after overnight fasting. The levels of blood glucose and the area under the curves (AUC) were determined as described for ITT and OGTT.

Histopathological examination and immunohistochemical staining. Samples of liver and abdominal white adipose tissue (WAT) were resected and fixed with 10% formaldehyde phosphate buffered saline (pH 7.4), then embedded in paraffin, sectioned, stained with haematoxylin/eosin (H&E stain), Oil Red O, or sirius red, and finally analyzed by Zeiss Imager A2-M2 microscope (Carl Zeiss AG, Cöttingen). Immunohistochemical staining of TGF-β1 in the liver was conducted, and observed

according to the method as described previously. [54] The average TGF-β1 area was calculated by Image J software.

Immunofluorescence of the liver TNFα. Liver was fixed with methanol and blocked using PBS with 5% BSA. For TNFα immunostaining, slides were incubated in PBS-BSA (PBS with 0.1% BSA) containing primary anti-TNFα antibody (1:200; Lifetechnologies) followed by an appropriate secondary antibody with anti-rabbit Alexa Fluor 610 (1:250; Invitrogen). Cell nuclei were stained with DAPI. Images were taken with Leica SP8 confocal microscope, and the expression level of TNFα for each cell were analyzed using Image J software.

Real-time qPCR analysis. Total RNA was prepared from liver and ileum tissues using TriPure Isolation Reagents (Roche). Quantification and integrity analysis of total RNA were performed by running 1 μL of each sample on an Agilent 2100 Bioanalyzer (Agilent RNA 6000 Nano Kit, Agilent). The cDNA was prepared by reverse transcription. The real-time qPCR was conducted with *Gapdh* mRNA as a housekeeping gene. Sequences of the primers used for real-time qPCR are available in the supplemental information (Table S1).

Distribution of polysaccharide in small intestinal. A method developed by Lebovitz*et al.* was used to determine the polysaccharide distribution in small intestine. [13] The *ob/ob* mice were sacrificed under ether anesthesia and the small intestines were resected. The intestine was segmented into nine sections from duodenum toileum, and then flushed with 5 ml ice-cold saline carefully. After centrifugation (8000 × g) at room tempurature for 30 minutes, the resulting supernatant was used for assay. A

commercial kit (GOD assay, Jiancheng Biological Engineering Institute, Najing, China) was used to determine the polysaccharide content of each intestine section. The absorbance was measured at 550 nm using a Spectra Max 190 microplate reader (Molecular Devices Inc.), and polted as in Figure S9E.

Transcriptome analysis. The samples for transcriptome analysis were prepared using Illumina's kit following manufacturer's protocol (Illumina, San Diego, CA, USA). The cDNA library was sequenced on the Illumina sequencing platform (HiSeqTM 2000), and two technical repetitions were performed. The raw reads were cleaned by eradicating adaptor sequences, empty reads and low quality sequences. RefSeq genome annotation and DESeq2 were applied for differential gene expression analysis. Functional annotation with gene ontology terms (http://www.geneontology.org) was conducted using Blast2Go software. The KEGG pathways annotation was performed using BLAST all against Kyoto Encycolpodia of Genes and Genomes database. The RNA sequencing data have been deposited in the National Center for Biotechnology Information GenBank repository (Accession numbers: SRX3512721-SRX3512726 for **7d**).

Microbiota analysis. DNA for gut microbiota analysis was extracted from about 150 mg caecum contents of *ob/ob* mice treated with **7d** by a previously reported method, [55] and subjected to 16S rRNA gene high-throughput sequencing using the Illumina HiSeq PE250 platform. The 16S rRNA gene V3-V4 region was amplified using the primers F341 (CCTACGGGRSGCAGCAG) and R806 (GGACTACVVGGGTATCTAATC). Chimeras were filtered using USEARCH, and

the remaining sequences were clustered to generate operational taxonomic units (OTUs) at 97% similarity. A representative sequence of each OTU was assigned to a taxonomic level in the RDP database using the RDP classifier. The 16S rRNA gene sequence data was processed using linear discriminant analysis effect size (LEfSe). LEfSe differences among biological groups were tested for significance using a non-parametric factorial Kruskal-Wallis sum-rank test followed by Wilcoxon rank-sum test. The 16S rRNA gene sequencing data have been deposited in the National Center for Biotechnology Information GenBank repository (Accession numbers: SRX3402443-SRX3402458 for **7d**).

SCFA analysis. Fecal samples were collected from animals after the treatment with **7d**. Each fecal sample was lyophilized, and then pestled using a mortar. Forty milligrams of the homogenic powders were extracted with 1 mL MeOH. After sonication, the samples were centrifuged, and the supernatants were used for GC-MS analysis. GC-MS was performed on a GCMS-QP2010 Ultra with an autosampler (SHIMADZU) and the Rtx-wax capillary column (60 m, 0.25 mm i.d., 0.25 μm film thickness; SHIMADZU). Oven temperature was programmed from 60 to 100 ºC at 5 ºC/min, with a 1-minute hold; to 150 ºC at 5 ºC/min, with a 5-minute hold; to 225 ºC at 30 ºC/min, with a 20-minute hold. Injection of a 2 μL sample was performed at 230 ºC. Helium, at a flow of 1.2 $mL \cdot min^{-1}$, was the carrier gas. Electronic impact was recorded at 70 eV.

Statistical analysis. For all analyses and for each group, any exclusion decision was made according to results obtained by the Grubbs test for outlier detection. All

results are expressed as mean ± SEM. For multiple comparisons, statistical analysis was performed using one-way or two-way ANOVA followed by the Tukey's multiple comparison tests with GraphPad 6.0. $P < 0.05$ was considered statistically significant.

Associated content

Supporting information

Additional experimental data for compound synthesis. HPLC assay for α-glucosidase inhibiton test. The chemical stability analysis, long-term toxicity, and additional PK data for **7d**. Anti-metabolic syndrome effects of **7d** in DIO mice. Effects of **7d** on the *in vivo* α-glucosidase inhibitory activitys and small intestinal carbohydrate distribution. Transcriptome analysis of the hepatic gene expression profile in **7d**-treated *ob/ob* mice. Effects of **7d** on antibiotics treated *ob/ob* mice. NMR spectra and molecular formula strings of related compounds. This content is available free of charge on ACS Publication website.

Corresponding Author

For Hongwei Liu: Phone: +86 10 64806074

E-mail: liuhw@im.ac.cn

Notes

The authors declare no competing financial interest.

Acknowledgements

We thank Jinwei Ren (State Key Laboratory of Mycology, Institute of Microbiology, Chinese Academy of Sciences) for his help in measuring the NMR

data. This work was financially supported by the National Natural Science Foundation of China (81773614), the Key Research Program of the Chinese Academy of Sciences (KFZD-SW-219) and Strategic Biological Resources Service Network programme of CAS (ZSTH-016), and the Youth Innovation Promotion Association of CAS (2014074).

Abbreviations

ALT: alanine aminotransferase, AST: aspartate transaminase, AUC: area under curves, CLGI: chronic low-grade inflammation, DIO: diet induced obesity, FFA: free fatty acids, GC-MS: gas chromatography-mass spectrometry, GO: gene-ontology, H&E: hematoxylin-eosin, HbA1c: glycated hemoglobin A1c, IBD: inflammatory bowel disease, ITT: insulin tolerance test, KEGG: Kyoto encyclopaedia of genes and genomes, LDA: linear discriminant analysis, LDL-C: low-density-lipoprotein-cholesterol, LEfSe: LDA effect size, LPS: lipopolysaccharide, MS: metabolic syndrome, NASH: nonalcoholic steatohepatitis, PK: pharmacokinetics, OGTT: oral glucose tolerance test, SCFAs: short-chain fatty acids, SEM: standard error of the mean, TC: total cholesterol, TG: triglycerides, TGF-β1: transforming growth factor-β1, TNF: tumor necrosis factor, WAT: white adipose tissue.

References

(1) Eckel, R.; Grundy, S. The the metabolic syndrome *Lancet* **2005**, *9468* (365), 1415-1428.

(2) Lu, J.; Wang, L.; Li, M.; Xu, Y.; Jiang, Y.; Wang, W.; Li, J.; Mi, S.; Zhang, M.; Li, Y.; Wang, T.; Xu, M.; Zhao, Z.; Dai, M.; Lai, S.; Zhao, W.; Wang, L.; Bi, Y.; Ning, G. Metabolic syndrome among adults in China: The 2010 China noncommunicable disease surveillance. *J. Clin. Endocr. Metab.* **2017**, *102* (2), 507-515.

(3) Peters, J. Polypharmacology - foe or friend? *J. Med. Chem.* **2013**, *56* (22), 8955-8971.

(4) Rodrigues, T.; Reker, D.; Schneider, P.; Schneider, G. Counting on natural products for drug design. *Nat. Chem.* **2016**, *8* (6), 531-541.

(5) Cragg, G. M.; Newman, D. J. Biodiversity: A continuing source of novel drug leads. *Pure Appl. Chem.* **2005**, *77* (1), 7-24.

(6) Lee, J.; Liu, J.; Feng, X.; Hernandez, M. A. S.; Mucka, P.; Ibi, D.; Choi, J. W.; Ozcan, U. Withaferin A is a leptin sensitizer with strong antidiabetic properties in mice. *Nat. Med.* **2016**, *22* (9), 1023-1032.

(7) Friesen, J. A.; Rodwell, V. W. The 3-hydroxy-3-methylglutaryl coenzyme-A (HMG-CoA) reductases. *Genome Biol.* **2004**, *5* (11), 248.

(8). Istvan, E. S.; Deisenhofer, J. Structural mechanism for statin inhibition of HMG-CoA reductase. *Science* **2001**, *292* (5519), 1160-1164.

(9) van de Laar, F. A.; Lucassen, P. L.; Akkermans, R. P.; van de Lisdonk, F. H.; Rutten, G. E.; van Weel, C. alpha-Glucosidase inhibitors for patients with type 2 diabetes - results from a cochrane systematic review and meta-analysis. *Diabetes Care* **2005**, *28* (1), 154-163.

(10) Lynch, S. V.; Pedersen, O. The human intestinal microbiome in health and disease. *New Engl. J. Med.* **2016**, *375* (24), 2369-2379.

(11) Shapiro, H.; Suez, J.; Elinav, E. Personalized microbiome-based approaches to metabolic syndrome management and prevention. *J. Diabetes* **2017**, *9* (3), 226-236.

(12) Brunkwall, L.; Orho-Melander, M. The gut microbiome as a target for prevention and treatment of hyperglycaemia in type 2 diabetes: from current human evidence to future possibilities. *Diabetologia* **2017**, *60* (6), 943-951.

(13) Lebovitz, H. E. Alpha-glucosidase inhibitors. *Endocrin. Metab. Clin.* **1997**, *26* (3), 539-542.

(14) Gu, Y.; Wang, X.; Li, J.; Zhang, Y.; Zhong, H.; Liu, R.; Zhang, D.; Feng, Q.; Xie, X.; Hong, J.; Ren, H.; Liu, W.; Ma, J.; Su, Q.; Zhang, H.; Yang, J.; Wang, X.; Zhao, X.; Gu, W.; Bi, Y.; Peng, Y.; Xu, X.; Xia, H.; Li, F.; Xu, X.; Yang, H.; Xu, G.; Madsen, L.; Kristiansen, K.; Ning, G.; Wang, W. Analyses of gut microbiota and plasma bile acids enable stratification of patients for antidiabetic treatment. *Nat. Comm.* **2017**, *8*, 1785.

(15) Zhang, X.; Fang, Z.; Zhang, C.; Xia, H.; Jie, Z.; Han, X.; Chen, Y.; Ji, L. Effects of acarbose on the gut microbiota of prediabetic patients: a randomized, double-blind, controlled crossover trial. *Diabetes Ther.* **2017**, *8* (2), 293-307.

(16) Su, B.; Liu, H.; Li, J.; Sunli, Y.; Liu, B.; Liu, D.; Zhang, P.; Meng, X. Acarbose treatment affects the serum levels of inflammatory cytokines and the gut content of *bifidobacteria* in Chinese patients with type 2 diabetes mellitus. *J. Diabetes* **2015**, *7* (5), 729-739.

(17) Wu, H.; Esteve, E.; Tremaroli, V.; Khan, M. T.; Caesar, R.; Manneras-Holm, L.; Stahlman, M.; Olsson, L. M.; Serino, M.; Planas-Felix, M.; Xifra, G.; Mercader, J. M.; Torrents, D.; Burcelin, R.; Ricart, W.; Perkins, R.; Fernandez-Real, J. M.; Backhed, F. Metformin alters the gut microbiome of individuals with treatment-naive type 2 diabetes, contributing to the therapeutic effects of the drug. *Nat. Med.* **2017**, *23* (7), 850-867.

(18) Zhang, X.; Zhao, Y.; Xu, J.; Xue, Z.; Zhang, M.; Pang, X.; Zhang, X.; Zhao, L. Modulation of gut microbiota by berberine and metformin during the treatment of high-fat diet-induced obesity in rats. *Sci. Rep.* **2015**, *5*, 14405.

(19) Wang, Y.; Shou, J.-W.; Li, X. Y.; Zhao, Z.-X.; Fu, J.; He, C.-Y.; Feng, R.; Ma, C.; Wen, B.-Y.; Guo, F.; Yang, X.-Y.; Han, Y.-X.; Wang, L. L.; Tong, Q.; You, X.-F.; Lin, Y.; Kong, W.-J.; Si, S.-Y.; Jiang, J.-D. Berberine-induced bioactive metabolites of the gut microbiota improve energy metabolism. *Metabolism* **2017**, *70*, 72-84.

(20) Ubeda, M.; Lario, M.; Munoz, L.; Borrero, M. J.; Rodriguez-Serrano, M.; Sanchez-Diaz, A.-M.; del Campo, R.; Lledo, L.; Pastor, O.; Garcia-Bermejo, L.; Diaz, D.; Alvarez-Mon, M.; Albillos, A. Obeticholic acid reduces bacterial translocation and inhibits intestinal inflammation in cirrhotic rats. *J. Hepatol.* **2016**, *64* (5), 1049-1057.

(21) Xu, J.; Chen, H.-B.; Li, S. L. Understanding the molecular mechanisms of the interplay between herbal medicines and gut microbiota. *Med. Res. Rev.* **2017**, *37* (5), 1140-1185.

(22) Sung, M. M.; Kim, T. T.; Denou, E.; Soltys, C. L. M.; Hamza, S. M.; Byrne, N. J.; Masson, G.; Park, H.; Wishart, D. S.; Madsen, K. L.; Schertzer, J. D.; Dyck, J. R. B. Improved glucose homeostasis in obese mice treated with resveratrol is associated with alterations in the gut microbiome. *Diabetes* **2017**, *66* (2), 418-425.

(23) Sanodiya, B. S.; Thakur, G. S.; Baghel, R. K.; Prasad, G. B. K. S.; Bisen, P. S. Ganoderma lucidum: a potent pharmacological macrofungus. *Curr. Pharm. Biotechno.* **2009**, *10* (8), 717-742.

(24) Wang, K.; Bao, L.; Ma, K.; Zhang, J.; Chen, B.; Han, J.; Ren, J.; Luo, H.; Liu, H. A novel class of alpha-glucosidase and HMG-CoA reductase inhibitors from *Ganoderma leucocontextum* and the anti-diabetic properties of ganomycin I in KK-A(y) mice. *Eur. J. Med. Chem.* **2017**, *127*, 1035-1046.

(25) Yajima, A.; Urao, S.; Katsuta, R.; Nukada, T. Concise syntheses and biological activities of ganomycin I and fornicin A. *Eur. J. Org. Chem.* **2014**, *4*, 731-738.

(26) Ballantyne, C. M.; Neutel, J.; Cropp, A.; Duggan, W.; Wang, E. Q.; Plowchalk, D.; Sweeney, K.; Kaila, N.; Vincent, J.; Bays, H. Results of Bococizumab, A monoclonal antibody against proprotein convertase subtilisin/kexin type 9, from a randomized, placebo-controlled, dose-ranging study in statin-treated subjects with hypercholesterolemia. *Am. J. Cardiol.* **2015**, *115* (9), 1212-1221.

(27) Stein, E. A.; Mellis, S.; Yancopoulos, G. D.; Stahl, N.; Logan, D.; Smith, W. B.; Lisbon, E.; Gutierrez, M.; Webb, C.; Wu, R.; Du, Y.; Kranz, T.; Gasparino, E.; Swergold, G. D. Effect of a monoclonal antibody to PCSK9 on LDL cholesterol. *New Engl. J. Med.* **2012**, *366* (12), 1108-1118.

(28) Rader, D. J. New therapeutic approaches to the treatment of dyslipidemia. *Cell Metab.* **2016**, *23* (3), 405-412.

(29) Wree, A.; Broderick, L.; Canbay, A.; Hoffman, H. M.; Feldstein, A. E. From NAFLD to NASH to cirrhosis - new insights into disease mechanisms. *Nat. Rev. Gastro. Hepat.* **2013**, *10* (11), 627-636.

(30) Meehan, C. J.; Beiko, R. G. A phylogenomic view of ecological specialization in the Lachnospiraceae, a family of digestive tract-associated Bacteria. *Genome Biol. Evol.* **2014**, *6* (3), 703-713.

(31) Manco, M.; Putignani, L.; Bottazzo, G. F. Gut microbiota, lipopolysaccharides, and innate immunity in the pathogenesis of obesity and cardiovascular risk. *Endocr. Rev.* **2010**, *31* (6), 817-844.

(32) Cani, P. D.; Bibiloni, R.; Knauf, C.; Neyrinck, A. M.; Neyrinck, A. M.; Delzenne, N. M.; Burcelin, R. Changes in gut microbiota control metabolic endotoxemia-induced inflammation in high-fat diet-induced obesity and diabetes in mice. *Diabetes* **2008**, *57* (6), 1470-1481.

(33) Uberos, J.; Molina-Carballo, A.; Fernandez-Puentes, V.; Rodriguez-Belmonte, R.; Munoz-Hoyos, A. Overweight and obesity as risk factors for the asymptomatic carrier state of *Neisseria meningitidis* among a paediatric population. *Eur. J. Clin. Microbiol.* **2010**, *29* (3), 333-334.

(34) Shen, F.; Zheng, R.-D.; Sun, X.-Q.; Ding, W.-J.; Wang, X.-Y.; Fan, J.-G. Gut microbiota dysbiosis in patients with non-alcoholic fatty liver disease. *Hepd. int.* **2017**, *16* (4), 375-381.

(35) Andoh, A.; Nishida, A.; Takahashi, K.; Inatomi, O.; Imaeda, H.; Bamba, S.; Kito, K.; Sugimoto, M.; Kobayashi, T. Comparison of the gut microbial community between obese and lean peoples using 16S gene sequencing in a Japanese population. *J. Clin. Biochem. Nutr.* **2016**, *59* (1), 65-70.

(36) Hardham, J. M.; King, K. W.; Dreier, K.; Wong, J.; Strietzel, C.; Eversole, R. R.; Sfintescu, C.; Evans, R. T. Transfer of Bacteroides splanchnicus to Odoribacter gen. nov as Odoribacter splanchnicus comb. nov., and description of Odoribacter denticanis sp nov., isolated from the crevicular spaces of canine periodontitis patients. *Int. J. Syst. Evol. Micr.* **2008**, *58*, 103-109.

(37) Kostic, A. D.; Chun, E.; Robertson, L.; Glickman, J. N.; Gallini, C. A.; Michaud, M.; Clancy, T. E.; Chung, D. C.; Lochhead, P.; Hold, G. L.; El-Omar, E. M.; Brenner, D.; Fuchs, C. S.; Meyerson, M.; Garrett, W. S. *Fusobacterium nucleatum* potentiates intestinal tumorigenesis and modulates the tumor-immune microenvironment. *Cell Host Microbe* **2013**, *14* (2), 207-215.

(38) Hamer, H. M.; Jonkers, D.; Venema, K.; Vanhoutvin, S.; Troost, F. J.; Brummer, R. J. Review article: the role of butyrate on colonic function. *Aliment. Pharm. Ther.* **2008**, *27* (2), 104-119.

(39) Diao, H.; Jiao, A. R.; Yu, B.; He, J.; Yu, J.; Zheng, P.; Huang, Z. Q.; Luo, Y. H.; Luo, J. Q.; Mao, X. B.; Chen, D. W, Stimulation of intestinal growth with distal ileal infusion of short-chain fatty acid: a reevaluation in a pig model. *Rsc Adv* **2017**, *7* (49), 30792-30806.

(40) Zhou, D.; Pan, Q.; Xin, F.-Z.; Zhang, R.-N.; He, C.-X.; Chen, G.Y.; Liu, C.; Chen, Y.W.; Fan, J.G. Sodium butyrate attenuates high-fat diet-induced steatohepatitis in mice by improving gut microbiota and gastrointestinal barrier. *World J. Gastroentero.* **2017**, *23* (1), 60-75.

(41) Li, Z.; Yi, C.-X.; Katiraei, S.; Kooijman, S.; Zhou, E.; Chung, C. K.; Gao, Y.; van den Heuvel, J. K.; Meijer, O. C.; Berbee, J. F. P.; Heijink, M.; Giera, M.; Willems van Dijk, K.; Groen, A. K.; Rensen, P. C. N.; Wang, Y. Butyrate reduces appetite and activates brown adipose tissue via the gut-brain neural circuit. *Gut*. DOI: 10.1136/gutjnl-2017-314050 (In press).

(42) Byndloss, M. X.; Olsan, E. E.; Rivera-Chavez, F.; Tiffany, C. R.; Cevallos, S. A.; Lokken, K. L.; Torres, T. P.; Byndloss, A. J.; Faber, F.; Gao, Y.; Litvak, Y.; Lopez, C. A.; Xu, G.; Napoli, E.; Giulivi, C.; Tsolis, R. M.; Revzin, A.; Lebrilla, C. B.; Baumler, A. J. Microbiota-activated PPAR-gamma signaling inhibits dysbiotic Enterobacteriaceae expansion. *Science* **2017**, *357* (6351), 570-582.

(43) Lee, S.; Lee, Y.; Kim, J.; An, J.; Kim, K.; Lee, H.; Kong, H.; Song, Y.; Kim, K. Atorvastatin and rosuvastatin improve physiological parameters and alleviate immune dysfunction in metabolic disorders. *Biochem. Bioph. Res. Co.* **2016**, *478* (3), 1242-1247.

(44) Ren, K.; Hu, B.; Zhao, M.; Tu, Y.; Xie, X.; Zhang, Z. Ruthenium-Catalyzed Oxidation of Allyl Alcohols with intermolecular hydrogen transfer: synthesis of alpha, beta-unsaturated carbonyl compounds. *J. Org. Chem.* **2014**, *79* (5), 2170-2177.

(45) Bunce, R. A.; Nammalwar, B. (+/-)-2-Aryl-2,3-dihydro-4(1H)-quinolinones by a tandem reduction-michael addition reaction. *J. Heterocyclic Chem.* **2011**, *48* (3), 613-619.

(46) Alam, M. P.; Jagodzinska, B.; Campagna, J.; Spilman, P.; John, V. C-O bond formation in a microfluidic reactor: high yield SNAr substitution of heteroaryl chlorides. *Tetrahedron Lett.* **2016**, *57* (19), 2059-2062.

(47) Vellakkaran, M.; Andappan, M. M. S.; Nagaiah, K.; Nanubolu, J. B., Direct Synthesis of gamma-keto sulfones from allylic alcohols: one-pot palladium(II)-catalyzed generation of enones followed by water-mediated 1,4-addition of organosulfinates. *Eur. J. Org. Chem.* **2016**, *21*, 3575-3583.

(48) Reddy, A. G. K.; Satyanarayana, G. Metal-Free Domino One-pot decarboxylative cyclization of cinnamic acid esters: synthesis of functionalized indanes. *J. Org. Chem.* **2016**, *81* (24), 12212-12222.

(49) Slagbrand, T.; Lundberg, H.; Adolfsson, H. Ruthenium-catalyzed tandem-isomerization/asymmetric transfer hydrogenation of allylic alcohols. *Chem. Eur. J.* **2014**, *20* (49), 16102-16106.

(50) Bartholomaeus, R.; Bachmann, J.; Mang, C.; Haustedt, L. O.; Harms, K.; Koert, U. Synthesis of the AB-ring pyranolactone substructure of granaticin A. *Eur. J. Org. Chem.* **2013**, 1, 180-190.

(51) Schmidt, B.; Audoersch, S.; Kunz, O. Stereoselective synthesis of 2Z,4E-configured dienoates through tethered ring closing metathesis. *Synthesis-Stuttgart* **2016**, *48* (24), 4509-4518.

(52) Sampson, T. R.; Debelius, J. W.; Thron, T.; Janssen, S.; Shastri, G. G.; Ilhan, Z. E.; Challis, C.; Schretter, C. E.; Rocha, S.; Gradinaru, V.; Chesselet, M. F.; Keshavarzian, A.; Shannon, K. M.; Krajmalnik-Brown, R.; Wittung-Stafshede, P.; Knight, R.; Mazmanian, S. K. Gut microbiota regulate motor deficits and neuroinflammation in a model of parkinson's disease. *Cell* **2016**, *167* (6), 1469-1480.

(53) Kang, M.; Mischel, R. A.; Bhave, S.; Komla, E.; Cho, A.; Huang, C.; Dewey, W. L.; Akbarali, H. I. The effect of gut microbiome on tolerance to morphine mediated antinociception in mice. *Sci. Rep.* **2017**, *7*, 42658.

(54) Li, Y.; Wang, W.; Jia, X.; Zhai, S.; Wang, X.; Wang, Y.; Dang, S. A targeted multiple antigenic peptide vaccine augments the immune response to self TGF-beta 1 and suppresses ongoing hepatic fibrosis. *Arch. Immunol. Ther. Ex.* **2015**, *63* (4), 305-315.

(55) Jiang, C. Y.; Dong, L.; Zhao, J.-K.; Hu, X.; Shen, C.; Qiao, Y.; Zhang, X.; Wang, Y.; Ismagilov, R. F.; Liu, S. J.; Du, W. High-throughput single-cell cultivation on microfluidic streak plates. *Appl. Environ. Microb.* **2016**, *82* (7), 2210-2218.

Figure Legend

Table 1. *α*-Glucosidase and HMG-CoA reductase inhibitory activities of **7a**-**7n**

Table 2. Pharmacokinetic parameters of **7d** in rats

Scheme 1. Synthesis of compounds **7a** – **7m**

Figure 1. Effects of **7d** on body weight and food intake in *ob/ob* mice.

Figure 2. Effects of **7d** on blood glucose level and insulin resistance.

Figure 3. Effects of **7d** on lipid metabolism.

Figure 4. Compound **7d** reverses hepatic steatosis and fibrosis in *ob/ob* mice.

Figure 5. *In vivo α*-glucosidase inhibitory activity of **7d** in *ob/ob* mice.

Figure 6. Compound **7d** modulates the composition of gut microbiota in *ob/ob* mice.

Figure 7. Compound **7d** improves endotoxemia, SCFAs, and intestinal mucosal barrier function in the *ob/ob* mice.

Table 1. α-Glucosidase and HMG-CoA reductase inhibitory activities of **7a-7n**

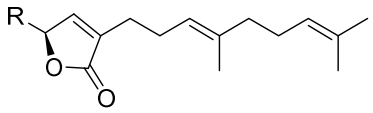

Compound		HMG-CoA reductase inhibition (IC_{50}, μM)	α-glucosidase inhibition (Small intestinal mucosa from rat) (IC_{50}, μM)
No.	-R		
7a		16.48±1.21	1.24±0.04
7b	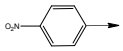	18.91±1.23	0.26±0.01
7c	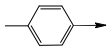	18.12±0.29	0.29±0.11
7d	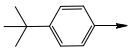	5.82±0.23	0.06±0.01
7e	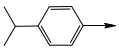	112.12±12.3	32.76±1.02
7f	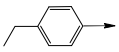	14.20±0.09	0.17±0.02
7g	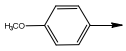	6.21±0.12	21.71±2.01
7h		7.43±0.13	5.11±0.21
7i		25.12±0.09	1.59±0.09
7j	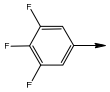	38.22±0.12	2.04±0.08
7k	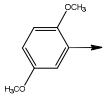	13.15±0.12	12.12±2.23
7l		8.90±1.09	19.28±1.02
7m		6.76±1.02	2.27±0.08
7n	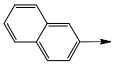	49.82±4.32	5.98±0.31
Ganomycin I	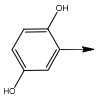	12.30±1.09	0.38±0.02
Positive control		Atorvastatin 0.93±0.03	Acarbose 1.26±0.02

Table 2. Pharmacokinetic parameters of **7d** in rats

NO.	Parameters (mean ± S.D)				
	C_{max} (ng/mL)	T_{max} (h)	AUC_{0-t} (ng/mL ×h)	$t_{1/2}$ (h)	$AUC_{0-\infty}$ (ng/mL ×h)
7d	49.3 ±8.6	7.0 ±1.7	274.0±42.3	1.8±0.6	280.2±44.9

Scheme 1. Synthesis of compounds **7a** – **7m**

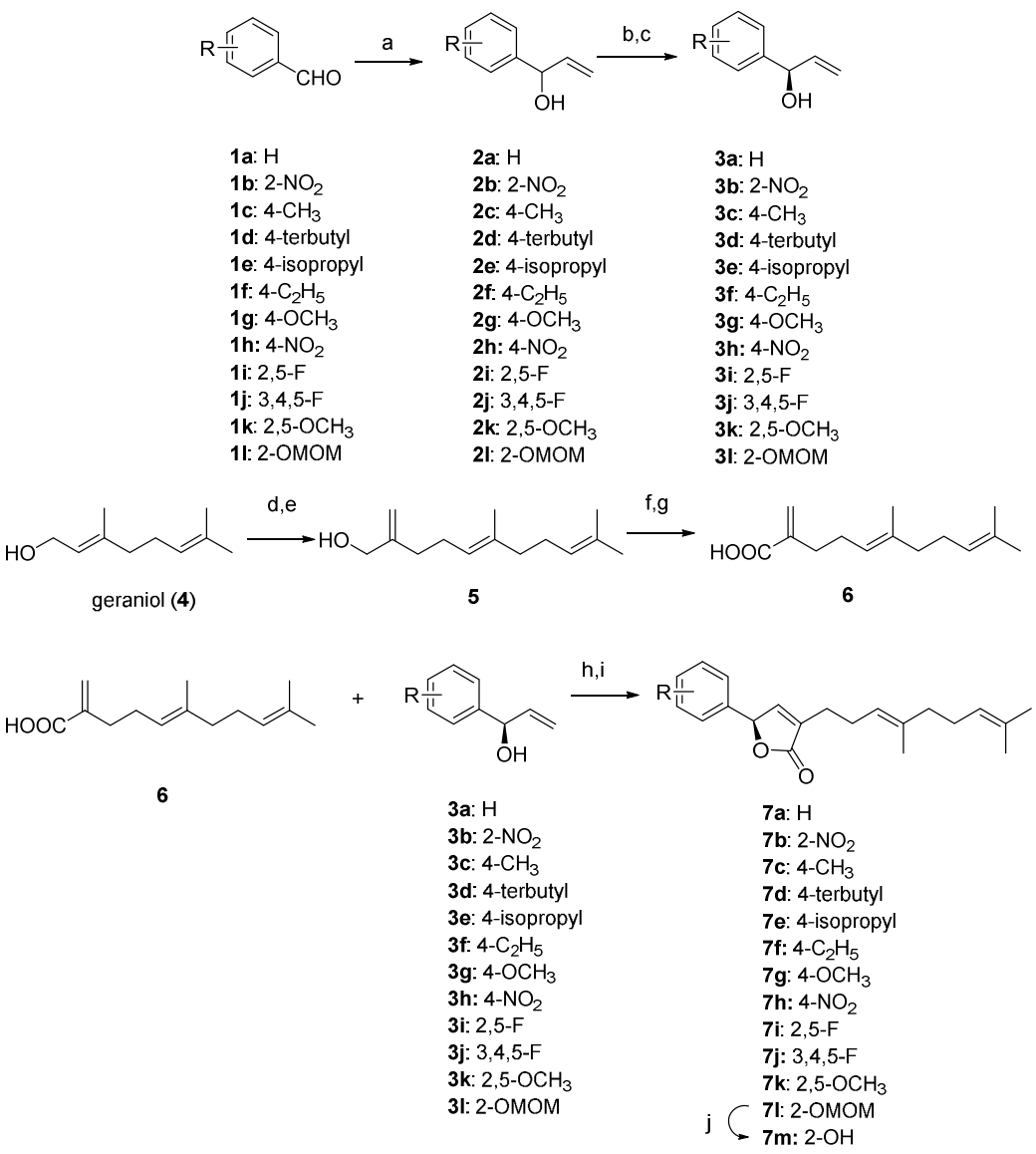

Reagents and conditions: (a) Allyl magnesium bromide, THF, -78 ºC to room temperature; (b) MnO_2, hexane, room temperature; (c) (*R*)-CBS catalyst (10 mol%), $BH_3{\cdot}SMe_2$, DCM, 20 ºC; (d) Ph_3P, CCl_4, reflux; (e) β-methallyl alcohol, nBuLi, TMEDA, Et_2O, -78 ºC to room temperature, then geranyl chloride; (f) MnO_2, hexane, room temperature; (g) $NaClO_2$, NaH_2PO_4,

2-methyl-2-butene, tBuOH, H_2O, 0 ºC to room temperature; (h) $Cl_3C_6H_2COCl$, DIPEA, DMAP, toluene, room temperature; (i) Grubbs 1st catalyst, CH_2Cl_2, room temperature; (j) TsOH, EtOH, room temperature. (DCM = dichloromethane, TMEDA = tetramethylethylenediamine, DIPEA = diisopropylefhylamine, DMAP = 4-(dimethylamino) pyridine, Grubbs 1st catalyst = $[(PCy_3)_2Cl_2Ru=CHPh]$

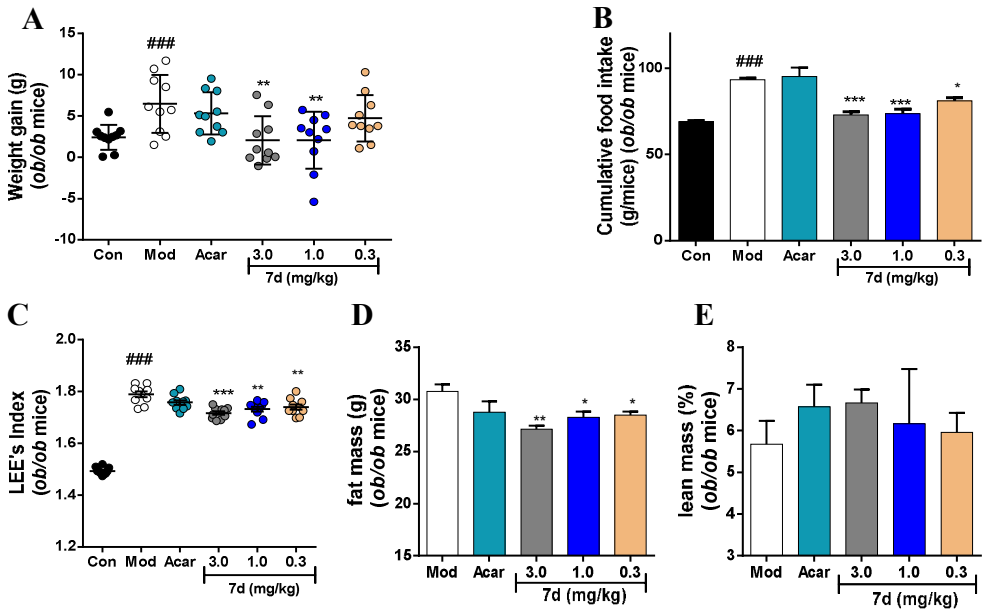

Figure 1. Effects of **7d** on body weight and food intake in *ob/ob* mice: (A) Body weight gain; (B) Cumulative food intake; (C) LEE index; (D) Fat mass; (E) Lean mass. Con, C57BL/6*J* mice control; Mod, *ob/ob* model; Acar, Acarbose 10.0 mg/kg. Data are presented as the mean ± standard error of the mean (SEM). N = 8-10 mice per group. Statistical analysis was done using one-way ANOVA followed by the Tukey post hoc test for A-F. * P<0.05; ** P<0.01; *** P<0.001.

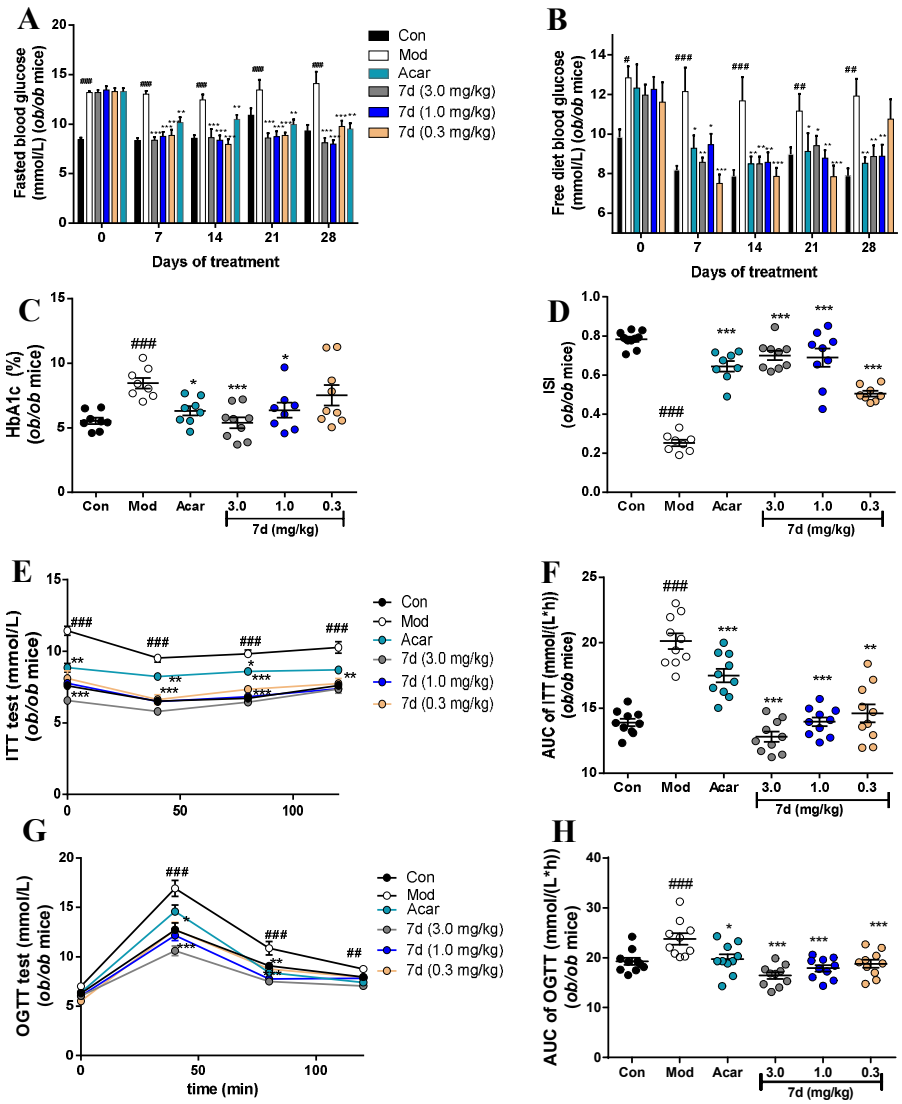

Figure 2. Effects of **7d** on blood glucose level and insulin resistance: (A) Free diet blood glucose in *ob/ob* mice; (B) Sequential monitoring of blood glucose in *ob/ob* mice after 4h fasting; (C) HbA1c in *ob/ob* mice; (D) ISI in *ob/ob* mice; (E) OGTT and (F) AUC on the 25th day of treatment in *ob/ob* mice; (G) ITT and (H) AUC on the 27th day of treatment in *ob/ob* mice. Con, C57BL/6*J* mice control; Mod, *ob/ob* model; Acar, Acarbose 10.0 mg/kg. Data are presented as the mean ± standard error of the mean (SEM). N = 8-10 mice per group. Statistical analysis was done using one-way ANOVA followed by the Tukey post hoc test for C, D, F, H, and two-way ANOVA followed by the Bonferroni post hoc test for A, B, E, G. * P<0.05; ** P<0.01; *** P<0.001.

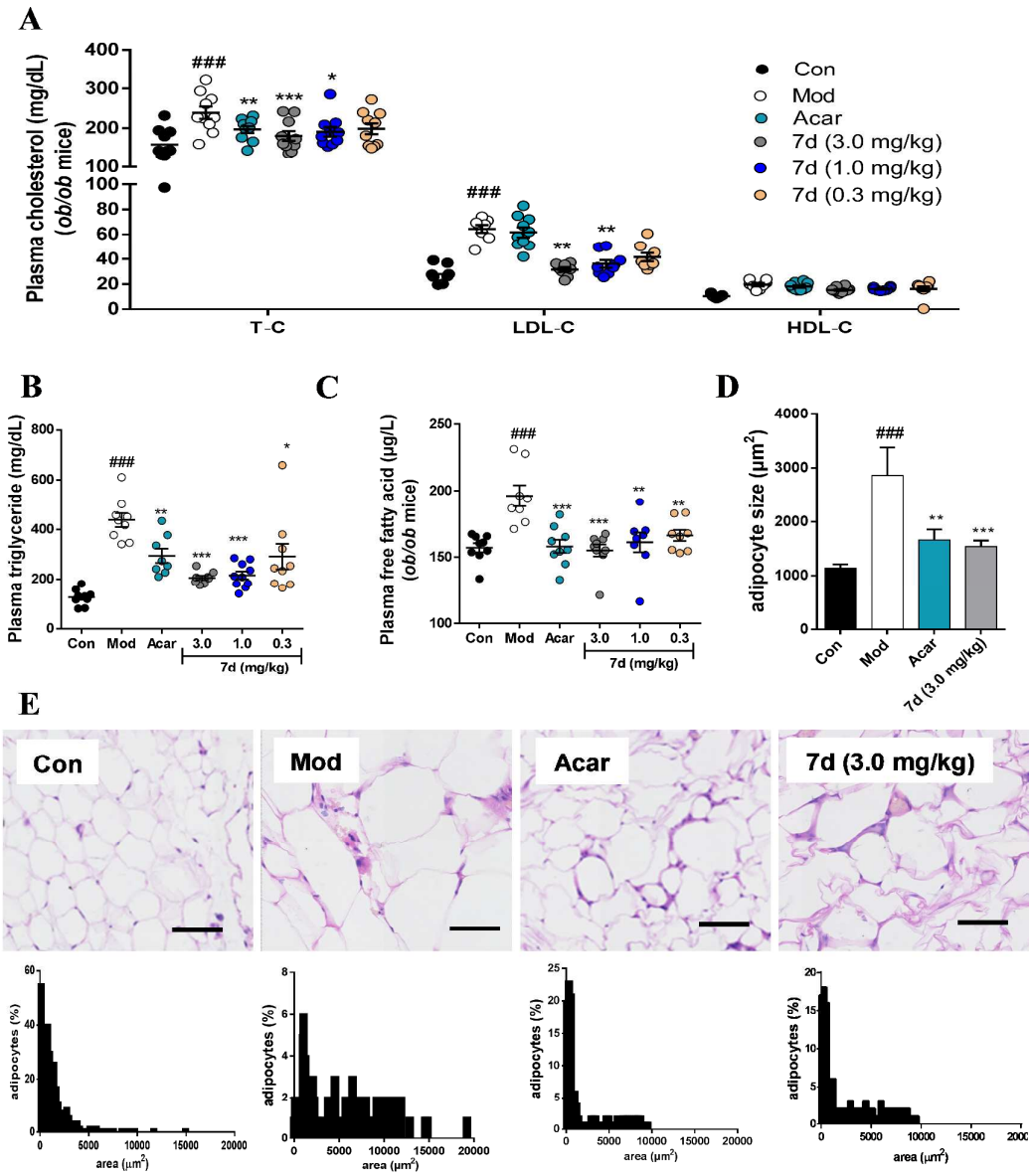

Figure 3. Effects of **7d** on lipid metabolism: (A) Plasma total cholesterol, LDL-C and HDL-C; (B) Plasma triglycerides; (C) Plasma free fatty acids; (D) Mean adipocyte size (3 mice per group); (E) Representative H&E-stained pictures and distribution of adipocyte size in WAT deposits (3 mice per group). Measurements were taken from distinct samples. Scale bars, 100 μm. Con, C57BL/6*J* mice control; Mod, *ob/ob* model; Acar, Acarbose 10.0 mg/kg. Data are presented as the mean ± standard error of the mean (SEM). N = 8-10 mice per group. Statistical analysis was done using one-way ANOVA followed by the Tukey post hoc test for A-C, E. * P<0.05; ** P<0.01; *** P<0.001.

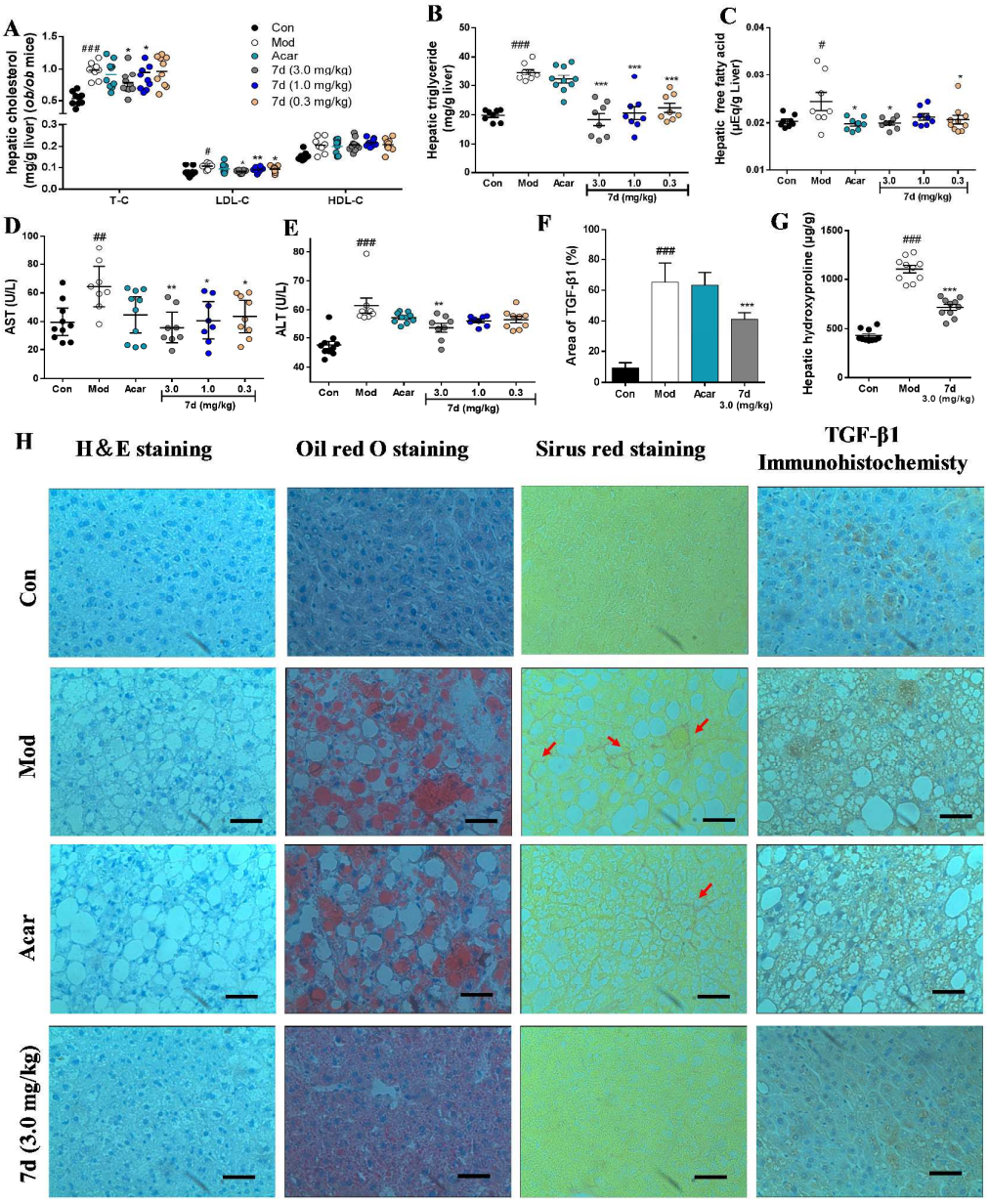

Figure 4. Compound **7d** reverses hepatic steatosis and fibrosis in *ob/ob* mice: (A) Hepatic total cholesterol, LDL-C and HDL-C; (B) Hepatic triglycerides; (C) Hepatic free fatty acids; (D) Plasma aspartate transaminase (AST); (E) Plasma alanine transaminase (ALT); (F) Average Area of TGF-β1; (G) Hepatic hydroxyproline content; (H) Representative images of H&E staining, Oil Red O staining, Sirius Red staining, and TGF-β1 immunohistochemistry staining of the liver (N

=3 mice per group). Scale bars, 100 μm. Measurements were taken from distinct samples. Con, C57BL/6*J* mice control; Mod, *ob/ob* model; Acar, Acarbose 10.0 mg/kg. Data are presented as the mean ± standard error of the mean (SEM). N = 8-10 mice per group. Statistical analysis was done using one-way ANOVA followed by the Tukey post hoc test for A-F. * $P<0.05$; ** $P<0.01$; *** $P<0.001$.

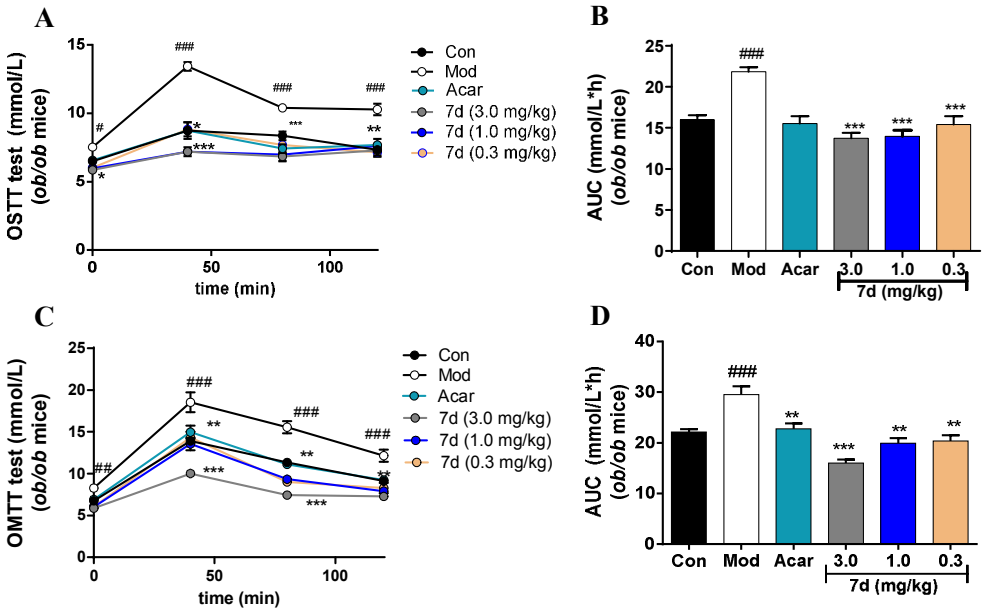

Figure 5. *In vivo* α-glucosidase inhibitory activity of **7d** in *ob/ob* mice: (A) OSTT test and (B) AUC on the 30th day of treatment in *ob/ob* mice; (C) OMTT test and (D) AUC on the 32th day of treatment in *ob/ob* mice. Con, C57BL/6*J* mice control; Mod, *ob/ob* model; Acar, Acarbose 10.0 mg/kg. Values are expressed as means ± SEM (n = 8-10 for *ob/ob* mice); *P<0.05, **P<0.01, ***P<0.001 versus *ob/ob* model group.

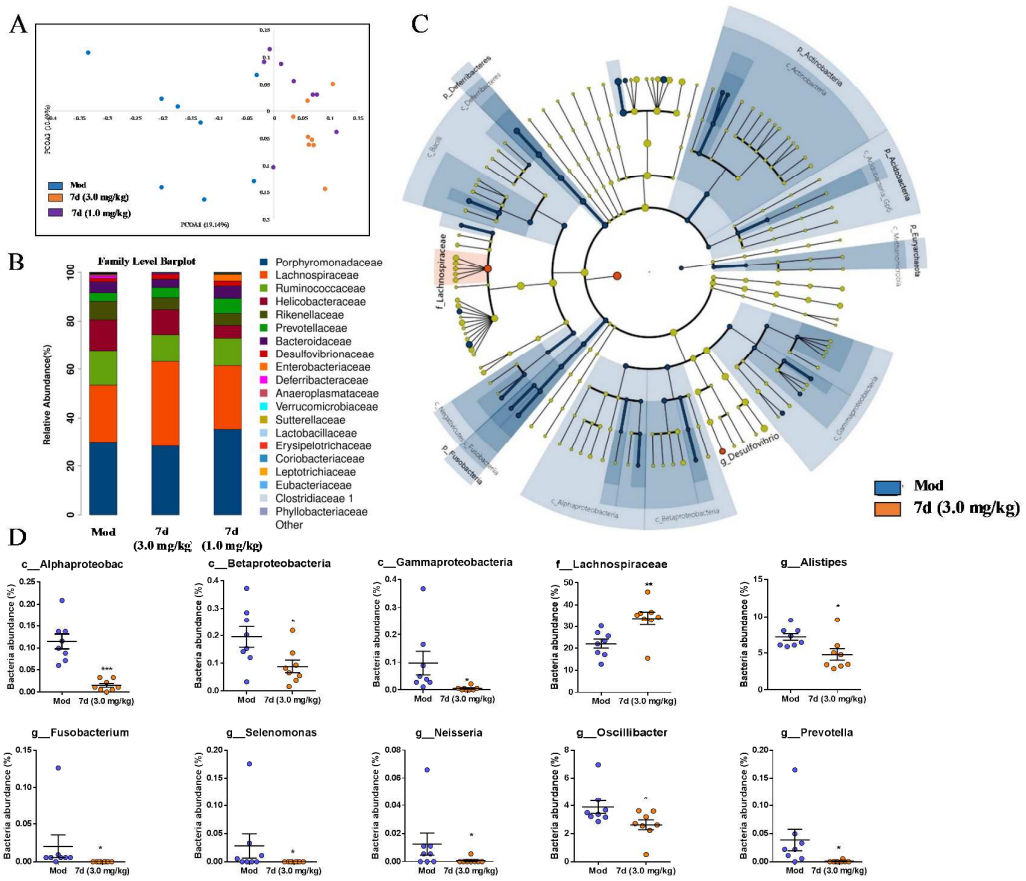

Figure 6. Compound **7d** modulates the composition of gut microbiota in *ob/ob* mice: (A) Nonmetric Multidimensional Scaling (NMDS) analysis with the Multi-response Permutation Procedures (MRPP) significance test; (B) Bacterial taxonomic profiling of intestinal bacteria from different groups at the family level; (C) Taxonomic cladogram generated from LEfSe analysis of 16S rRNA gene sequences. Blue color indicates enriched taxa in the vehicle-treated group. Orange color represents enriched taxa in the **7d**-treated group. Each circle's size is proportional to the taxon's abundance; (D) Comparison of the taxonomic abundance among the indicated groups. N = 8 mice per group. Data are presented as the mean ± SEM. The statistical significance in bacterial abundance among the different samples was assessed by the ANOSIM test. * P<0.05; ** P<0.01; *** P<0.001.

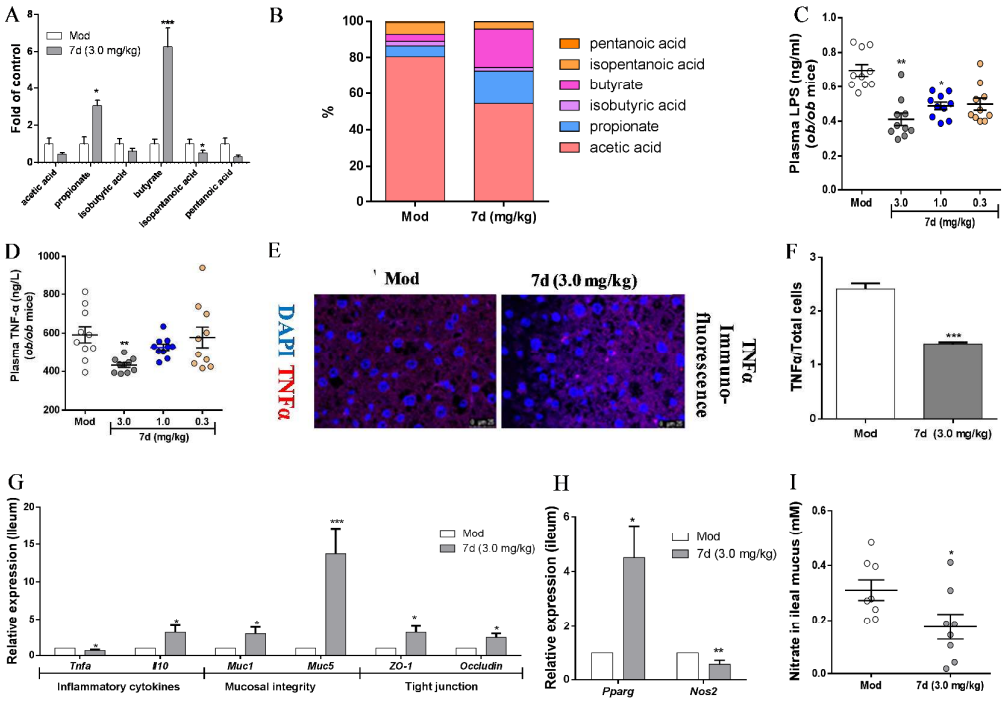

Figure 7. Compound **7d** improves endotoxemia, SCFAs, and intestinal mucosal barrier function in the *ob/ob* mice; (A) Levels and (B) composition of short chain fatty acids (SCFAs) in the faecal samples; (C) Plasma levels of LPS, n =10; (D) Plasma levels of TNFα by ELISA; (E) Representative immunofluorescence staining images of TNFα in liver (N = 3 mice per group); (F) Average area of TNFα per cell; (G) mRNA expression of genes *Tnfa*, *Il10*, *Muc-1*, *Muc-5*, *ZO-1*, and *Occludin* in the ileum; (H) mRNA expression of genes *Pparg* and *Nos2* in the ileum; (I) Concentration of nitrate in the colonic mucus layer. Mod, *ob/ob* model. Values are expressed as means ± SEM (n = 10 for *ob/ob* mice); *P<0.05, **P<0.01, ***P<0.001 versus *ob/ob* model group.

Graphic abstract